SAND81-7026
Unlimited Release
UC-60

Fixed Wake Analysis of the Darrieus Rotor

R. E. Wilson, S. N. Walker
Oregon State University, Corvallis, Oregon 97331

Prepared by Sandia National Laboratories, Albuquerque, New Mexico 87185 and Livermore, California 94550 for the United States Department of Energy under Contract DE-AC04-76DP00789

Printed July 1981

Prepared for Sandia National Laboratories Under Contract #42-2967

Sandia National Laboratories

SF 2900-Q(3-80)

Issued by Sandia National Laboratories, operated for the United States Department of Energy by Sandia Corporation.

NOTICE: This report was prepared as an account of work sponsored by an agency of the United States Government. Neither the United States Government nor any agency thereof, nor any of their employees, nor any of their contractors, subcontractors, or their employees, makes any warranty, express or implied, or assumes any legal liability or responsibility for the accuracy, completeness, or usefulness of any information, apparatus, product, or process disclosed, or represents that its use would not infringe privately owned rights. Reference herein to any specific commercial product, process, or service by trade name, trademark, manufacturer, or otherwise, does not necessarily constitute or imply its endorsement, recommendation, or favoring by the United States Government, any agency thereof or any of their contractors or subcontractors. The views and opinions expressed herein do not necessarily state or reflect those of the United States Government, any agency thereof or any of their contractors or subcontractors.

Printed in the United States of America

Available from
National Technical Information Service
U. S. Department of Commerce
5285 Port Royal Road
Springfield, VA 22161

NTIS price codes
Printed copy: $7.00
Microfiche copy: A01

Distribution
Category UC-60

SAND81-7026
Unlimited Distribution
Printed November 1980

FIXED WAKE ANALYSIS OF THE DARRIEUS ROTOR

R. E. Wilson
S. N. Walker

Oregon State University
Mechanical Engineering Department
Corvallis, Oregon 97331

ABSTRACT

Development and validation of a Darrieus wind turbine aerodynamic performance prediction model is described. Using a fixed-wake approach, the model combines some of the more desirable features of vortex/lifting line and conservation of momentum/streamtube approaches. The model thus accounts for up- and downwind differences that are predicted by vortex approaches while retaining the short computer run times found with streamtube models. The model treats the effects of stall, curved blades, blade pitch, and blade attachment location. Results agree with those obtained with Sandia National Laboratories' 17-m-diameter Darreius VAWT.

Prepared for the Sandia National Laboratories Under Contract No. 42-2967

TABLE OF CONTENTS

	Page
SUMMARY	vii
OBJECTIVE	ix
APPROACH	xi
CHAPTER 1 - THE QUASI-STEADY AERODYNAMICS OF A PITCHING AIRFOIL	1
CHAPTER 2 - POWER	11
CHAPTER 3 - INDUCED VELOCITY	18
CHAPTER 4 - VORTEX RELATIONS	21
CHAPTER 5 - DARRIEUS ROTOR TEST DATA	27
CHAPTER 6 - ANALYTICAL RESULTS	31
REFERENCES	37
APPENDIX A - COMPUTER PROGRAM	38
APPENDIX B - LINEAR AERODYNAMICS	46
APPENDIX C - GEOMETRY	52
APPENDIX D - DRAG COEFFICIENT	54

SUMMARY

A Darrieus rotor performance prediction model using a fixed wake approach has been developed and is operational. The model combines some of the best features of vortex and streamtube approaches in that it accounts for fore-and-aft differences that are predicted by vortex approaches while retaining the low run times associated with streamtube theory. The analysis treats the effects of stall, curved blades, blade pitch and blade attachment location.

The results have been compared to test data from the 17 meter Sandia rotor. Agreement is good.

OBJECTIVE

The objective of this contract is to reduce Darrieus Rotor Cost-of-Electricity (COE) using passive aerodynamic schemes. COE is governed by the energy capture and the machine cost. Increased aerodynamic performance increases energy capture, however, as the results of current Sandia tests yield measured power coefficients over 0.40 (up to 0.46) it appears that improvements in COE will come from decreasing machine cost rather than increasing aerodynamic output.

Reductions in the machine cost come about in several ways in which aerodynamics plays a significant role. These are:

1. Increasing Rotor Rpm. The gearbox represents a significant fraction of the total machine cost. By increasing rotor rpm, peak gearbox torque and therefore gearbox cost can be reduced.

2. Decreasing $K_p)_{Max}$. Critical and expensive components of the rotor are sized by the maximum output of the rotor which occurs at $K_p)_{Max}$. The maximum rotor output occurs at high speeds where the total hours of rotor are small. There are two penalties incurred by a rotor which has a high value of $K_p)_{Max}$.

   First, the drive train and generator must be larger. This increases the cost part of the COE both in the initial investment and in the operation and maintenance term.

Secondly, since the gearbox and generator are oversized, the energy losses associated with partial load operation are greater. Net energy production in light winds is reduced. Additionally the total annual hours of operation is reduced.

3. Decrease Service Factors. Because of the lack of certainty concerning the value of $K_p)_{Max}$ and the lack of availability of gearboxes and generators in a continuum of sizes, the drive train and generator that are installed in a Darrieus Rotor will have a rating above that required to accommodate $K_p)_{Max}$. The ratio of installed capacity to required capacity is the service factor. While some margin of safety is desirable, reduction of service factors can decrease COE for the reasons given in item 2. Such reductions require increased confidence in predicting $K_p)_{Max}$.

APPROACH

The approach to tailoring the C_p curve to reduce the cost of energy involves the adjustment of the aerodynamic configuration of the rotor blades. The rotor chord, pitch and airfoil section are the principal variables, however, with the use of extruded blades, local variations in chord size are not possible. Blade pitch and camber are then the variables that will be examined to tailor the rotor performance to decrease the COE.

Machine costs can be determined from the Sandia Optimization Code for a given rotor configuration while the rotor performance curve must be generated from an aerodynamic analysis.

The initial step that we have taken is the development of a simple, inexpensive model for aerodynamic performance of a Darrieus Rotor. The following six chapters detail the development and comparison of the theory to test data.

CHAPTER 1

THE QUASI-STEADY AERODYNAMICS OF A PITCHING AIRFOIL

In this chapter, the aerodynamic forces and moments acting on a pitching airfoil are derived. The force system is found to consist of three parts: The Kutta-Joukowski force acting at quarter chord; a leading edge suction force; and a moment. The effective angles of attack for evaluation of this Kutta-Joukowski force includes the pitching velocity at the three-quarter chord point, however, the angle at which the Kutta-Joukowski force acts does not include the pitching velocity.

Consider a right cylinder as shown below in Figure 1-1. The coordinates x,y are locked in the cylinder which is rotating with angular velocity Ω and translating with velocities U_x and U_y. By transforming the cylinder (actually a flat plate) into a circle,

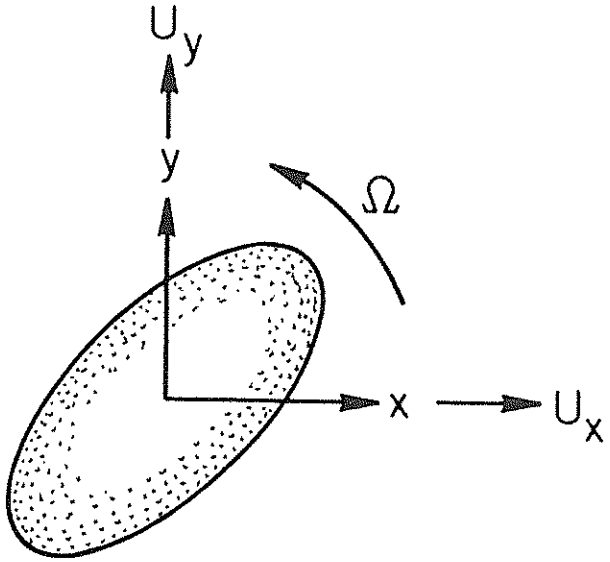

Figure 1-1 - Moving Cylinder

the complex potential may be written using the boundary function (1). Letting the complex velocity $Q = U_x - iU_y$, the boundary function $B(z)$ is given by

$$B(z) = Qz - \bar{Q}\bar{z} - i\Omega z\bar{z}$$

Transforming to the circle plane, $z = f(\zeta)$ and we obtain

$$B(\zeta) = Qf(\zeta) - \bar{Q}\bar{f}(\zeta) - i\Omega f(\zeta)\bar{f}(\zeta)$$

With the transformation $z = \zeta + r^2/\zeta$, where $r = c/4$, the airfoil of chord c is transformed into a circle of radius c/4. Using the above transform

$$B(\zeta) = Q(\zeta + \frac{r^2}{\zeta}) - \bar{Q}(\bar{\zeta} + \frac{r^2}{\bar{\zeta}}) - i\Omega(\zeta + \frac{r^2}{\zeta})(\bar{\zeta} + \frac{r^2}{\bar{\zeta}})$$

on the circle $\zeta\bar{\zeta} = r^2$ so that the boundary function becomes

$$B(\zeta) = (Q - \bar{Q})(\zeta + \frac{r^2}{\zeta}) - i\Omega(\zeta + \frac{r^2}{\zeta})^2$$

which indeed is a function of ζ alone. Now the boundary function $B_1(\zeta)$ contains only the negative powers of ζ and is equal to the complex potential. Thus

$$B_1(\zeta) = W(\zeta) = (Q - \bar{Q})\frac{r^2}{\zeta} - i\Omega\frac{r^4}{\zeta^2}$$

If there is circulation, we may add a vortex at the origin (cw is positive) giving

$$W(\zeta) = (Q - \bar{Q})\frac{r^2}{\zeta} + \frac{i\Gamma}{2\pi}\ln\zeta - i\Omega\frac{r^4}{\zeta^2}$$

The complex velocity in the circle plane is

$$q \equiv \frac{dW}{d\zeta}$$

and in the cylinder (airfoil) plane

$$q = \frac{dW}{dz} = \frac{dW}{d\zeta}\frac{1}{dz/d\zeta} = \frac{dW}{d\zeta}\frac{1}{1-r^2/\zeta^2}$$

Thus, noting $Q - \bar{Q} = -2iU_y$

$$q = [2iU_y + \frac{i\Gamma}{2\pi\zeta} + 2i\Omega\frac{r^4}{\zeta^3}]/(1 - r^2/\zeta^2)$$

At the trailing edge $\zeta = r$, we employ the Kutta condition. Thus the bracketed term must vanish and we obtain the value of Γ required to meet the Kutta condition.

$$\Gamma = -\pi cU_y - \pi\frac{\Omega c^2}{4}$$

Let the system velocities be as shown in Figure 1-2. The airfoil as illustrated is now rotating about Point A.

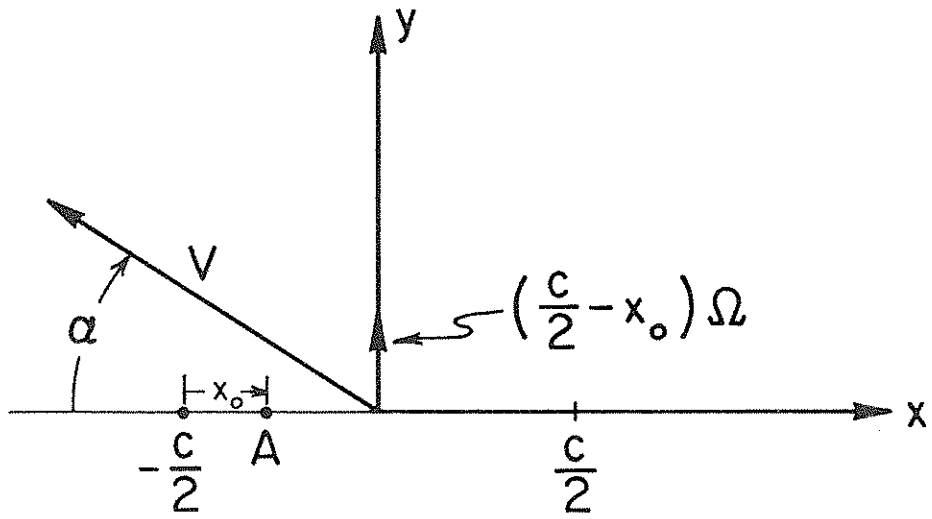

Figure 1-2 - System Velocities

From the figure, it may be seen that

$$U_y = V \sin\alpha + c\Omega(\frac{1}{2} - \frac{x_o}{c})$$

Substituting into the expression for the circulation

$$\Gamma = -(\pi c V \sin\alpha + \pi c^2 \Omega(\frac{3}{4} - \frac{x_o}{c}))$$

or

$$\Gamma = -\pi c(V \sin\alpha + c\Omega(\frac{3}{4} - \frac{x_o}{c}))$$

where the bracketed term is the velocity normal to the airfoil at the three-quarter chord position.

The force on the airfoil may be determined from the extended Blasius Theorem. Using the formulation developed in (1) and neglecting wake terms, the conjugate force is given by

$$\bar{F} \equiv X - iY = i\rho Q\Gamma - \Omega\rho \int_C \bar{z}\, d\bar{W}$$

where the integral is evaluated over the airfoil contour. Now letting

$$\bar{I}_2 = \int_C z dW = \int_C z \frac{dW}{d\zeta} d\zeta$$

$$\bar{I}_2 = \int_C (\zeta + \frac{r^2}{\zeta})[2iU_y \frac{r^2}{\zeta^2} + \frac{i\Gamma}{2\pi\zeta} + 2i \frac{\Omega r^4}{\zeta^3}]d\zeta$$

Since the airfoil contour in the ζ plane is a circle, the result is simply the residue or

$$\bar{I}_2 = -4\pi r^2 U_y = -\frac{\pi c^2}{4} U_y = I_2$$

Thus

$$\bar{F} = i\rho\Gamma Q + \rho \frac{\pi c^2}{4} \Omega U_y$$

From Figure 1-2

$$Q = U_x = iU_y = -V \cos\alpha - iV \sin\alpha - ic\Omega(\frac{1}{2} - \frac{x_o}{c})$$

or

$$Q = -V e^{i\alpha} - ic\Omega(\frac{1}{2} - \frac{x_o}{c})$$

The conjugate force is

$$\bar{F} = -i\rho V\,\Gamma e^{i\alpha} + \rho c\Omega\left(\frac{1}{2} - \frac{x_o}{c}\right) + \rho\frac{\pi c^2}{4}\,\Omega U_y$$

The first term shall be called the Kutta-Joukowski force, $\bar{F}_{KJ}$. The line of action of this force is $-ie^{i\alpha}$ so F_{KJ} acts along $(\overline{-ie^{i\alpha}})$. Now

$$-ie^{i\alpha} = e^{i(\alpha+3\pi/2)} = e^{i(\alpha-\pi/2)}$$

so that

$$F_{KJ} = \rho V\Gamma e^{-i(\alpha-\pi/2)} = \rho V(-\Gamma)e^{-i(\alpha+\pi/2)}$$

In Figure 1-3, the directions are illustrated. For this case Γ is negative.

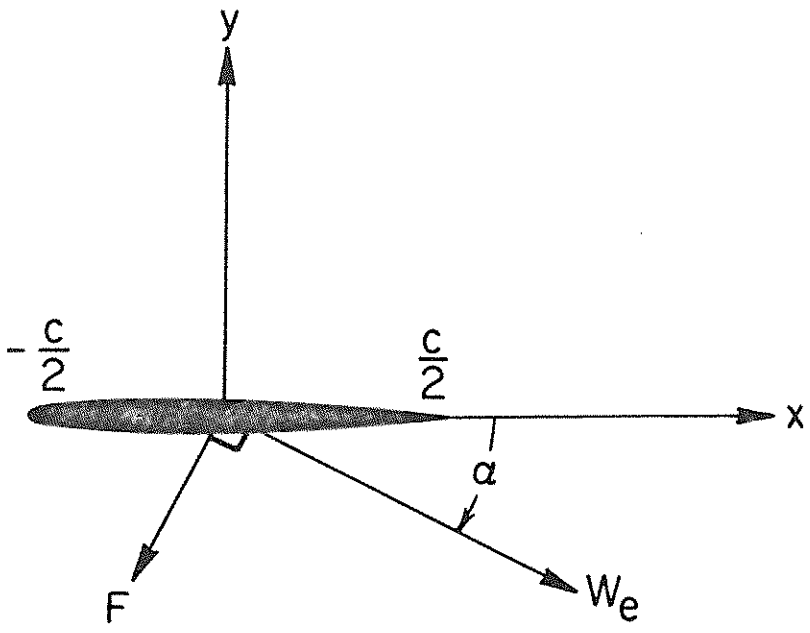

Figure 1-3 - Kutta-Joukowski Force

The velocity W_e is observed to be the velocity relative to the airfoil rather than the velocity of the airfoil through the static fluid.

The remaining terms of the conjugate force are real indicating that they must arise from leading edge suction. Calling these terms F_T where F_T acts in the (-x) direction

$$F_T \equiv -\rho\Omega\left(\frac{\pi c^2}{4} U_y + c\left(\frac{1}{2} - \frac{x_o}{c}\right)\Gamma\right)$$

or

$$F_T = -\rho \frac{\pi c^2}{4} \Omega\left[U_y - \left(\frac{1}{2} - \frac{x_o}{c}\right)(4U_y + c\Omega)\right]$$

and since

$$U_y = V \sin\alpha + c\Omega\left(\frac{1}{2} - \frac{x_o}{c}\right) = -W_e \sin\alpha + c\Omega\left(\frac{1}{2} - \frac{x_o}{c}\right)$$

which becomes

$$F_T = \rho\frac{\pi c^2\Omega}{4}\left[\left(1 - \frac{4x_o}{c}\right)W_e \sin\alpha + c\Omega\left(1 - 2\frac{x_o}{c}\right)^2\right]$$

A moment also acts on the airfoil. Again using the extended Blasius Theorem neglecting unsteady terms, the moment about the origin (ccW+) is

$$M = \text{Real}\left[\rho Q \int_c z\,dW\right] = \rho Q_{\text{Real}} \frac{\pi c^2}{4} U_y$$

where $Q_{Real} = -V \cos\alpha = -W_e \cos\alpha$.

Expressing U_y in terms of Γ

$$M = \rho W_e \cos\alpha \, (-\Gamma) \frac{c}{4} - \rho W_e \cos\alpha \frac{\pi c^3 \Omega}{16}$$

The first term is a counterclockwise moment (recall Γ is negative for this case) about the origin due to the Kutta-Joukowski force (i.e., F_{KJ} c/4 $\cos\alpha$). This shows that this force acts at c/4. The second term is a pure clockwise moment. The resulting forces on the airfoil are illustrated below, where

$$M_{c/4} = \rho W_e \cos\alpha \frac{\pi c^3 \Omega}{16}$$

Generalizing the results to a Darrieus Rotor blade that is situated at angle γ with respect to the axis of rotation of the rotor, the forces and moments are as shown in Figure 1-4. The

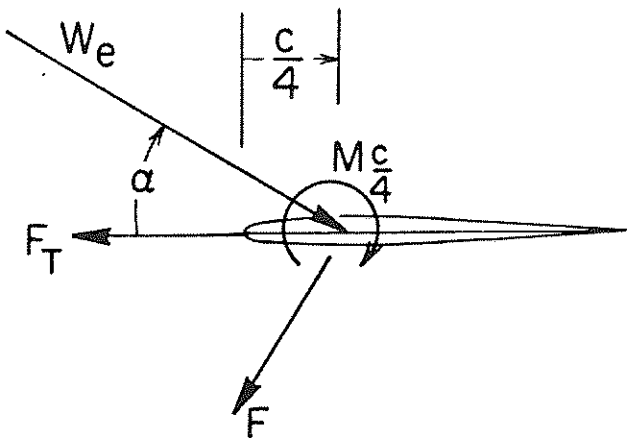

Figure 1-4 - Aerodynamic Loading of a Pitching Airfoil

individual terms may be determined from

$$F_{KJ} = \frac{1}{2} \rho W_e^{\ 2} \ cC_L \ (\alpha_E)$$

$$\alpha_E = \tan^{-1} \left(\frac{W_e \sin\alpha + c\Omega \cos\gamma (\frac{3}{4} - \frac{x_o}{c})}{W_e \cos\alpha} \right)$$

$$F_T = \rho \frac{\pi c^2}{4} \Omega \cos\gamma [(1 - \frac{4x_o}{c}) W_e \sin\alpha + c\Omega \cos\gamma (1 - \frac{2x_o}{c})^2]$$

$$M_{c/4} = \rho W_e \cos\alpha \frac{\pi c^3}{16} \Omega \cos\gamma$$

The effective angle of attack, α_E, is observed to include the pitching velocity at the three-quarter chord position.

When the airfoil is pitched at angle β as shown in Figure 1-5,

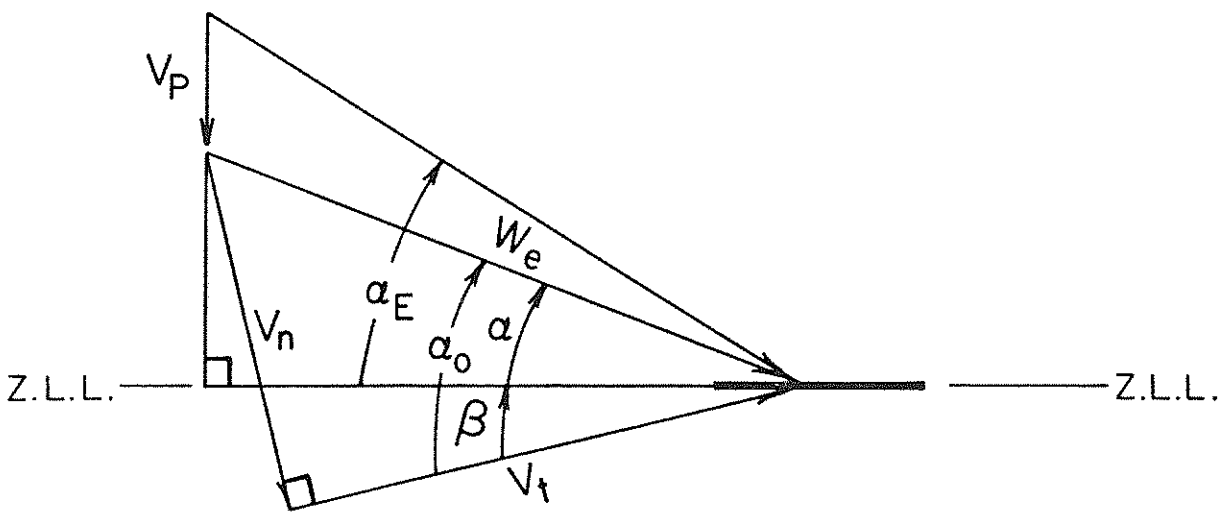

Figure 1-5 - Pitching Airfoil at Angle β

the loading may be further generalized. Using the zero lift line of the airfoil as a reference, the angles α, α_o, α_E and β are defined.

Since Darrieus Rotor velocities are usually given in terms of V_n and V_t, the effective angle of attack, α_E, which includes the pitching velocity, $c\Omega\cos\gamma(3/4 - x_o/c)$, will be expressed in terms of these velocities.

$$\tan\alpha_E = \frac{V_p + W_e\sin\alpha}{W_e\cos\alpha} = \frac{V_p + V_n\cos\beta - V_t\sin\beta}{V_t\cos\beta + V_n\sin\beta}$$

The loadings become:

$$F_{KJ} = \frac{1}{2}\rho W_e^2\, cC_L(\alpha_E)$$

$$F_T = \rho\frac{\pi c^2}{4}\Omega\cos\gamma[(1 - \frac{4x_o}{c})W_e\sin(\alpha_o - \beta) + c\Omega\cos\gamma(1 - \frac{2x_o}{c})^2]$$

$$M_{c/4} = \rho W_e\cos(\alpha_o - \beta)\frac{\pi c^3}{16}\Omega\cos\gamma$$

CHAPTER 2

POWER

The local torque developed on a Darrieus Rotor blade element is derived considering contributions from lift, drag and moment. The Kutta-Joukowski term is the only wake-producing term and thus controls the power.

Consider an element of a Darrieus Rotor blade as shown in Figure 2-1.

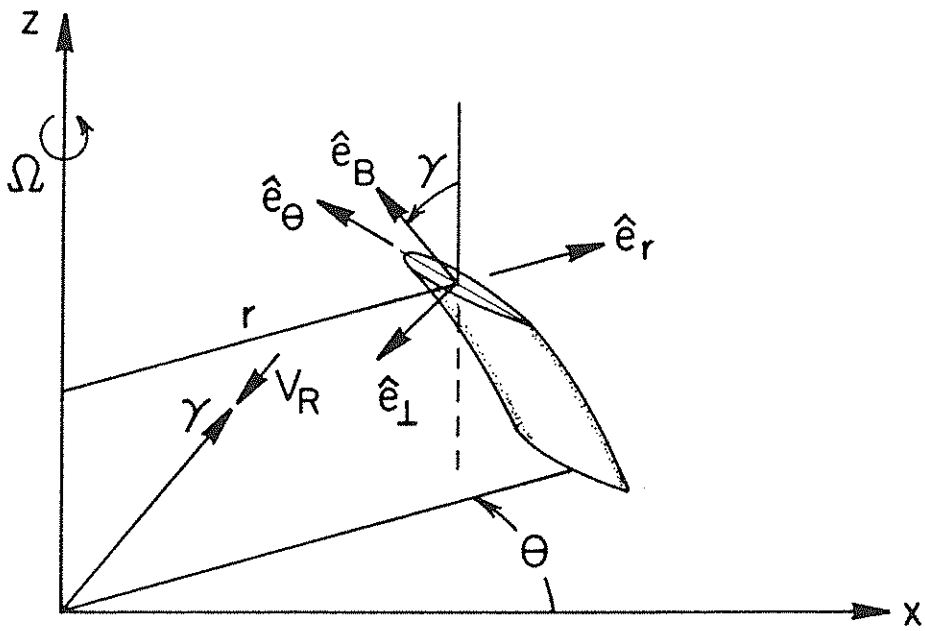

Figure 2-1 - Darrieus Rotor Blade Geometry

The local unit vectors may be expressed in terms of the unit vectors $\hat{i}$, $\hat{j}$, $\hat{k}$;

$$\hat{e}_r = \hat{i}\cos\theta + \hat{j}\sin\theta$$
$$\hat{e}_\theta = -\hat{i}\sin\theta + \hat{j}\cos\theta$$
$$\hat{e}_\perp = -\hat{e}_r\cos\gamma - \hat{k}\sin\gamma$$
$$\hat{e}_B = \hat{k}\cos\gamma - \hat{e}_r\sin\gamma$$

The blade rotates counterclockwise about the z axis. In order to determine the local effective wind on the airfoil, W_e, we define the following local velocities;

Local relative velocity due to rotation	$-r\Omega\hat{e}_\theta$
Local wind	$-V_a\hat{j}$

The relative velocity is given by

$$\vec{W} = -r\Omega\hat{e}_\theta - V_a\hat{j}$$

The spanwise component does not contribute to the lift or drag, so

$$\vec{W}_e = (\vec{W}\cdot\hat{e}_\theta)\hat{e}_\theta + (\vec{W}\cdot\hat{e}_\perp)\hat{e}_\perp$$

or

$$\vec{W}_e = -(r\Omega + V_a\cos\theta)\hat{e}_\theta + (V_a\sin\theta\cos\gamma)\hat{e}_\perp$$

So we find that

$$V_t = r\Omega + V_a\cos\theta = V_R(\frac{r}{R}X + (1 - a_i)\cos\theta_i)$$

$$V_n = V_a\sin\theta\cos\gamma = V_R(1 - a_i)\sin\theta_i\cos\gamma$$

where

$$V_a \equiv V_R(1 - a_i) \text{ and } X \equiv (R\Omega/V_R)$$

From Chapter 1 we find that

$$\tan\alpha_E = \frac{\cos\gamma(\frac{c}{R})X(\frac{3}{4} - \frac{x_o}{c}) + (1-a_i)\sin\theta_i\cos\gamma\cos\beta - (\frac{r}{R}X + (1-a_i)\cos\theta_i)\sin\beta}{(\frac{r}{R}X + (1-a_i)\cos\theta_i)\cos\beta + (1-a_i)\sin\theta_i\cos\gamma\sin\beta}$$

$$\tan\alpha_o = \frac{\cos\gamma\sin\theta_i(1-a_i)}{\frac{r}{RX} + (1-a_i)\cos\theta_i}$$

and

$$(\frac{W_e}{V_R})^2 = (\frac{r}{R}X + (1 - a_i)\cos\theta)^2 + \cos^2\gamma\sin^2\theta_i(1 - a_i)^2$$

The loading on the airfoil is shown in Figure 2-2.

An element of blade of length ds with differential loading as shown develops a torque dQ about the axis of rotation.

$$dQ = -dM\hat{e}_B\cdot\hat{k} + \{\vec{L} \times [\hat{e}_t dF_t + \hat{e}_{KJ}dF_{KJ} + \hat{e}_w dF_D]\}\cdot\hat{k}$$

where

$$\hat{e}_t = \hat{e}_\theta\cos\beta - \hat{e}_\perp\sin\beta$$
$$\hat{e}_{KJ} = \hat{e}_\perp\cos\alpha_o + \hat{e}_\theta\sin\alpha_o$$
$$\hat{e}_W = \hat{e}\sin\alpha_o - \hat{e}_\theta\cos\alpha_o$$
$$\vec{L} = r\hat{e}_r + c(\frac{x_o}{c} - \frac{1}{4})\hat{e}_t = r\hat{e}_r + c^*\hat{e}_t$$

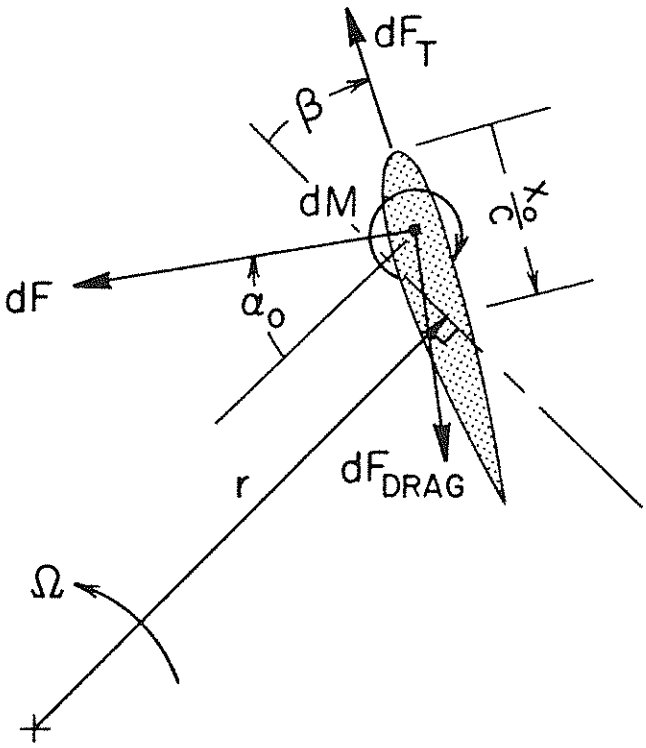

Figure 2-2 - Blade Loads

The torque may be rewritten as

$$dQ = dQ_M + dQ_t + dQ_{KJ} + dQ_D$$

where

$$dQ_M = -dM \cos\gamma = -\frac{dM}{ds} ds \cos\gamma = -dz \frac{dM}{ds}$$

$$dQ_M = -\rho W_e \cos(\alpha_o - \beta) \frac{\pi c^3}{16} \Omega \cos\gamma \, dz$$

$$dQ_t = (\bar{L} \times \hat{e}_t) \cdot \hat{k} \frac{dF_t}{ds} ds$$

$$= (\hat{e}_r \times \hat{e}_t) \cdot \hat{k} r \frac{dF_t}{ds} ds$$

$$= r\cos\beta \frac{dF_t}{ds} ds$$

Thus, the leading edge term F_t yields a torque

$$dQ_t = r\cos\beta\ \rho\frac{\pi c^2\Omega}{4}[(1 - 4\ \frac{x_o}{c})W_e\sin(\alpha_o - \beta) + c\Omega\cos\gamma(1 - 2\ \frac{x_o}{c})^2]dz$$

The Kutta-Joukowski contribution is

$$dQ_{KJ} = (\vec{L} \times \hat{e}_{KJ})\cdot k\ \frac{dF_{KJ}}{ds}\ ds$$

$$= (r\sin\alpha_o + c^*\cos\gamma\ \cos(\alpha_o - \beta))\ \frac{dF_{KJ}}{ds}\ ds$$

$$dQ_{KJ} = \frac{1}{2}\ \rho\ W_e^2 cC_L(\alpha_E)\ \frac{r\sin\alpha_o dz}{\cos\gamma} + \frac{1}{2}\ \rho\ W_e^2 cC_L(\alpha_E)c^*\cos(\alpha_o - \beta)dz$$

Finally the drag yields

$$dQ_D = (\vec{L} \times \hat{e}_w)\cdot\hat{k}\ dF_D = (-r\cos\alpha_o + c^*\cos\gamma\ \sin(\alpha_o - \beta))dF_p$$

$$dQ_D = -\ \frac{1}{2}\ \rho\ W_e^2 cC_D(\alpha_E)\ \frac{r\cos\alpha_o dz}{\cos\gamma} + \frac{1}{2}\ \rho\ W_e^2 cC_D(\alpha_E)c^*\sin(\alpha_o - \beta)dz$$

The blade circulation, Γ, is given by

$$\Gamma = -\pi c(V_n \cos\beta - V_t \sin\beta + c\Omega(\frac{3}{4} - \frac{x_o}{c})\cos\gamma)$$

As the wind speed goes to zero, the circulation does not go to zero. The remaining circulation is the bound circulation Γ_B. Since the bound circulation leaves no wake, it cannot do any net work. The Kutta-Joukowski term includes the bound circulation term. We shall determine the torque produced by the bound circulation and subtract it from the net torque in order to insure that no net work is produced by this term.

As the wind speed goes to zero

$$\Gamma_B \rightarrow \pi c r \Omega \sin\beta - \pi c^2 \Omega(\frac{3}{4} - \frac{x_o}{c})\cos\gamma$$

The instantaneous torque produced is

$$\frac{dQ_B}{ds} = B\hat{k}\cdot[\vec{r} \times \rho(\vec{W}_e \times \vec{\Gamma}_B)]$$

using the vector triple product and noting that $\Gamma_B = -\Gamma_B \hat{e}_B$

$$\frac{dQ_B}{dz} = -\rho B r \Gamma_B V_a \sin\theta_i$$

where $V_a = V_R(1 - a_i)$

Thus for arbitrary lift curve slope, C_{L_α}, we obtain

$$\frac{DQ_B}{Dz} = -C_{L_\alpha}\left(\frac{Bc}{R}\right)X\left(\frac{r}{R}\right)(1-a_i)\sin\theta_i\left[\left(\frac{r}{R}\right)\sin\beta-\left(\frac{c}{R}\right)\cos\gamma\left(\frac{3}{4}-\frac{x_o}{c}\right)\right]$$

where $\quad \frac{DQ}{Dz} \equiv \frac{dQ}{dz}\frac{1}{\frac{1}{2}\rho V_R^2 R^2}$

Summing the total of the other terms for B blades and subtracting the contribution of the bound circulation and adding a contribution from $C_M(\alpha_E)$ yields

$$\frac{DQ}{Dz} = \left\{\begin{array}{l}
\left(\frac{W_e}{V_R}\right)^2\left(\frac{Bc}{R}\right)\left(\frac{r}{R}\right)\left[\frac{C_L(\alpha_E)\sin\alpha_o - C_D(\alpha_E)\cos\alpha_o}{\cos\gamma}\right] \\[2ex]
\left(\frac{W_e}{V_R}\right)^2 B\left(\frac{c}{R}\right)^2\left(\frac{x_o}{c}-\frac{1}{4}\right)\left[C_L(\alpha_E)\cos(\alpha_o-\beta)+C_D(\alpha_E)\sin(\alpha_o-\beta)\right] \\[2ex]
\left(\frac{W_e}{V_R}\right)B\left(\frac{c}{R}\right)^2 X\frac{\pi}{2}\left(\frac{r}{R}\right)\left(1-\frac{4x_o}{c}\right)\sin(\alpha_o-\beta) \\[2ex]
B\left(\frac{c}{R}\right)^3 X^2\frac{\pi}{2}\left(\frac{r}{R}\right)\left(1-\frac{2x_o}{c}\right)^2\cos\gamma \\[2ex]
-B\left(\frac{W_e}{V_R}\right)\left(\frac{c}{R}\right)^3 X\frac{\pi}{8}\cos(\alpha_o-\beta)\cos\gamma \\[2ex]
\left(\frac{W_e}{V_R}\right)^2 B\left(\frac{c}{R}\right)^2 C_M(\alpha_E) \\[2ex]
\left(\frac{Bc}{R}\right)\left(\frac{r}{R}\right)X(1-a)\sin\theta\left[\left(\frac{r}{R}\right)C_L(\beta)-2\pi\left(\frac{c}{R}\right)\cos\gamma\left(\frac{3}{4}-\frac{x_o}{c}\right)\right]
\end{array}\right.$$

At first glance it would appear that there are a great number of power terms. In practice, only the Kutta-Joukowski term (devoid of bound circulation) produces any wake. Thus, the remaining terms are cosmetic and can be ignored unless instantaneous torques are required.

CHAPTER 3

INDUCED VELOCITY

In order to determine the power, the local value of a is required. Let us use a streamtube approach and equate the windwise momentum change to the mean blade force.

The streamtube is illustrated in Figure 3-1.

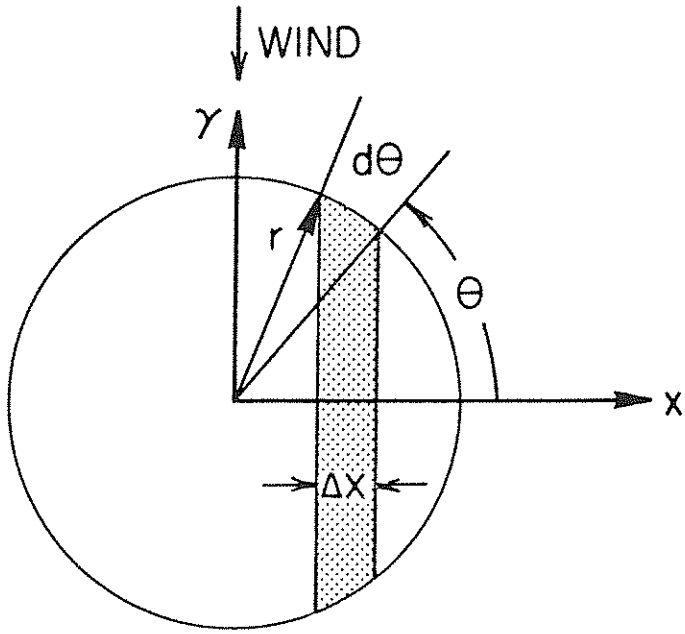

Figure 3-1 - Streamtube

Here $\Delta x = r d\theta |\sin\theta|$.

So

$$d\vec{F}\cdot\hat{j} = \rho\bar{V}_a r|\sin\theta|d\theta dz\ \Delta V_a,\ \Delta V_a<0$$

The blade force is

$$(d\vec{L}_F \cdot \hat{j} + d\vec{L}_R \cdot \hat{j})\frac{Bd\theta}{2\pi}$$

Now the leading edge suction terms do not contribute to the mean wake, thus

$$d\vec{L} \cdot \hat{j} = \frac{1}{2}\rho W_e^2 C_L c \frac{ds}{\cos\gamma}[\cos\alpha_o \hat{e}_\perp + \sin\alpha_o \hat{e}_\theta] \cdot \hat{j}$$

$$= -\frac{1}{2}\rho W_e^2 C_L c \frac{dz}{\cos\gamma}(\cos\alpha_o \sin\theta\cos\gamma - \sin\alpha_o \cos\theta)$$

Expanding

$$W_e \cos\alpha_o \cos\gamma \sin\theta = (r\Omega + V_a \cos\theta)\sin\theta\cos\gamma$$
$$-W_e \sin\alpha_o \cos\theta = -(V_a \sin\theta)\cos\theta\cos\gamma$$

so that

$$d\vec{L} \cdot \hat{j} = -\frac{1}{2}\rho W_e C_L c dz\ r\Omega\sin\theta$$

and

$$\frac{Bd\theta}{2\pi}(d\vec{L}_i \cdot \hat{j}) = -\frac{1}{2}\rho W_{e_i} C_{L_i} c\ r\Omega\sin\theta_i\ dz\ \frac{d\theta}{2\pi}$$

Now the momentum change is

$$d\vec{F}_y \cdot \hat{j} = -2\rho V_R^2 r|\sin\theta|a(1-a)d\theta dz$$

Equating the momentum change to the blade force where the momentum change is a function of a and blade force depends upon $a_{Local}(a_F$ or $a_R)$

$$-2\rho V_R^2|\sin\theta|a(1-a)rd\theta dz=-Bc\frac{d\theta}{2\pi}\frac{\rho V_R^2}{2}\frac{r}{R}X\quad\{\frac{W_{e_F}}{V_R}C_{L_F}\sin\theta_F+\frac{W_{e_R}}{V_R}C_{L_R}\sin\theta_R\}$$

canceling common terms

$$4a(1-a)|\sin\theta|=\frac{Bc}{R}X[\frac{C_{L_F}}{2\pi}\frac{W_{e_F}}{V_R}\sin\theta_F+\frac{C_{L_R}}{2\pi}\frac{W_{e_R}}{V_R}\sin\theta_R]$$

Since $\sin\theta_F \geq 0$, $\sin\theta_R = -\sin\theta_F$

$$a(1-a)=\frac{BcX}{4R}[\frac{C_{L_F}}{2\pi}\frac{W_{e_F}}{V_R}-\frac{C_{L_R}}{2\pi}\frac{W_{e_R}}{V_R}]$$

Here the effects of the bound circulation cancel (i.e., $\Gamma = \frac{c}{2}C_L W$).

CHAPTER 4

VORTEX RELATIONS

Now we proceed to obtain a relation between a_F and a_R. Consider an airfoil traversing the path shown. Between A and B the airfoil moves parallel to the free stream and generates no force. At point B, the airfoil suddenly changes direction and moves across the wind, generating both lift and circulation. Again at point C, the direction of motion is changed and vorticity is again shed, although the sign of shed vorticity is opposite that shed at B. The wake system that is generated is illustrated. The magnitude of the local circulation is shown. The direction is indicated by the arrows. We may take certain liberties with the illustrated path without changing the wake pattern.

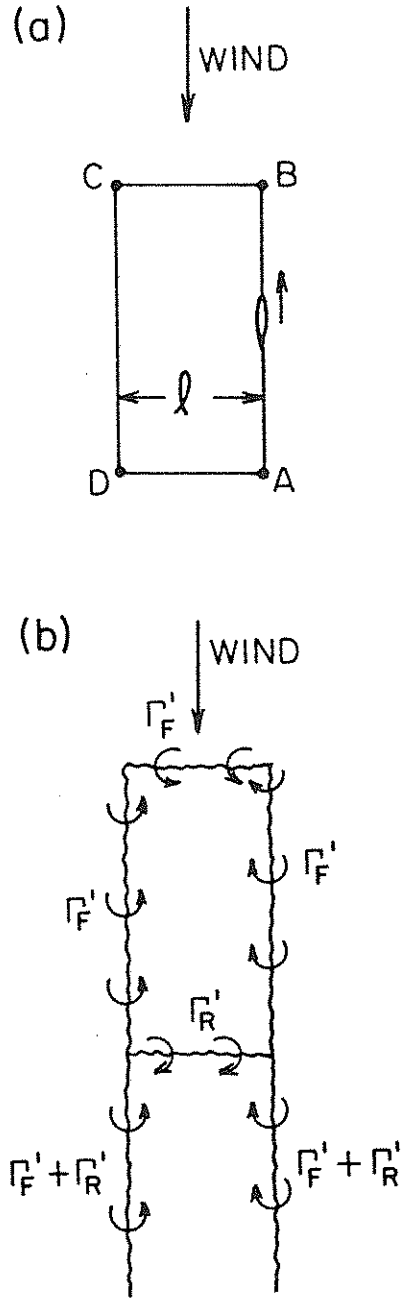

Figure 4-1 - Airfoil and Vorticity

In Figure 4-2 at the right, the distance ℓ has been reduced relative to the distance AB and the paths BC and DA have been made to conform with the path of a Darrieus Rotor blade. Thus, we have a streamtube of a Darrieus Rotor. Considering the flow in other streamtubes to be similar, we arrive at several "theorems."

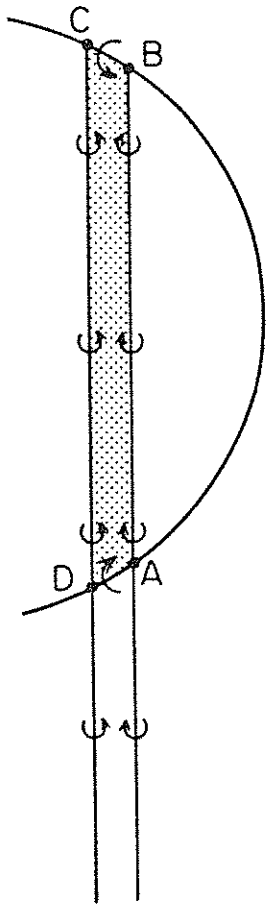

Figure 4-2 - Darrieus Streamtube

1. Since the flow along BC is influenced only by the flow inside the vortex street shed by BC, we have "independence of the elements."
2. As the streamtube gets smaller in width the wake from BC appears as a semi-infinite vortex street. The resulting induced velocity at the front is due only to the semi-infinite wake of the front, i.e., $\Delta U_F \sim \Gamma'_F$ <u>only</u>.
3. The rear station "sees" an infinite wake due to Γ'_F and a semi-inifinite wake due to Γ'_R. The rear all depends upon both Γ'_R and Γ'_F.

In analytical terms we may write

$$\Delta u_F = k_1 |\Gamma'_F| = a_F V_R$$

and

$$\Delta u_R = k_2 (2|\Gamma'_F| + |\Gamma'_R|) = a_R V_R$$

In the far wake

$$u_{Wake} = k_3 (2|\Gamma'_F| + 2|\Gamma'_R|) = 2a_W V_R$$

Here k relates vortex spacing and strengths. When the finite airfoils become a continuum of airfoils, all the k_i are equal and we obtain

$$\Delta u_R - \Delta u_F = k(|\Gamma'_F| + |\Gamma'_R|) = \frac{u_w}{2}$$

or

$$a_R - a_F = \frac{a_W}{2} \equiv a$$

and $$\frac{\Delta u_F}{\Delta u_R} = \frac{|\Gamma'_F|}{2|\Gamma'_F| + |\Gamma'_R|} = \frac{a_F}{a_R}$$

Using uniform sign convention for Γ', positive circulation being counterclockwise, one obtains

$$\frac{a_R}{a_F} = 2 - \frac{\Gamma'_R}{\Gamma'_F}$$

and

$$a_R - a_F = a$$

These relations are exactly the same as developed by Holme in this 1976 paper.* There remains the proper indentification of Γ'. The circulation to be used involves only the shed vorticity. Hence if we denote the total circulation by Γ_T and the bound circulation by Γ_B, then

$$\Gamma' = \Gamma_T - \Gamma_B$$

Bound circulation arises from several sources. If the blade is pitched at angle β as shown, there is a bound circulation

$$\Gamma_B)_\beta = -\frac{c}{2} r\Omega \, C_L(\beta)$$

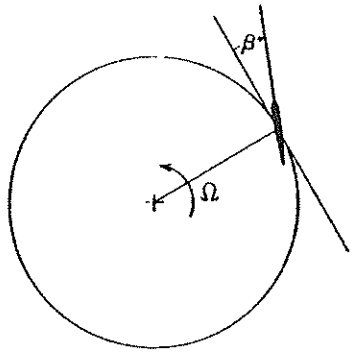

Figure 4-3 - Blade Pitch Angle

From Chapter 1, the bound circulation due to pitching is

*Holme, O. "A Contribution to the Aerodynamic Theory of the Vertical-Axis Wind Turbine," BHRA International Symposium on Wind Energy Systems, 9/76.

$$\Gamma_B)_\Omega = \pi c^2 \Omega \cos\gamma \left(\frac{3}{4} - \frac{x_o}{c}\right)\left(\frac{C_{L_\alpha}}{2\pi}\right)$$

Thus with $m = C_{L_\alpha}/2\pi$

$$\Gamma' = \Gamma_T - m\pi c^2 \Omega \cos\gamma \left(\frac{3}{4} - \frac{x_o}{c}\right) + \frac{c}{2} r\Omega C_L(\beta)$$

making Γ' dimensionless

$$\Gamma' \equiv \frac{\Gamma'}{V_R R} = \Gamma_T - m\pi \left(\frac{c}{R}\right)^2 X \cos\gamma \left(\frac{3}{4} - \frac{x_o}{c}\right) + \frac{c}{R}\frac{r}{R} X \frac{C_L(\beta)}{2}$$

$$\Gamma_T = \frac{c}{2} C_L W_e, \quad \Gamma_T = \frac{1}{2}\frac{c}{R}\frac{W_e}{V_R} C_L$$

Thus

$$\frac{\Gamma'_F}{\Gamma'_R} = \frac{\frac{W_{e_F}}{V_R} C_{L_F} - C_{L_\alpha}\frac{c}{R} X \cos\gamma \left(\frac{3}{4} - \frac{x_o}{c}\right) + \frac{r}{R} X C_L(\beta)}{\frac{W_{e_R}}{V_R} C_{L_R} - C_{L_\alpha}\frac{c}{R} X \cos\gamma \left(\frac{3}{4} - \frac{x_o}{c}\right) + \frac{r}{R} X C_L(\beta)}$$

as $\sin\theta \to 0$ $\quad \frac{W_{e_i}}{V_R} \to \frac{rX}{R} \pm (1-a_i)$

$$C_L = C_L(\alpha_E - \beta) \to 2\pi m\left[\frac{\cos\gamma X \frac{c}{R}\left(\frac{3}{4} - \frac{x_o}{c}\right)}{\frac{r}{R}X \pm (1-a_i)} - \beta\right]$$

$$\frac{\Gamma'_F}{\Gamma'_R} \to \frac{\mp 2\pi m(1-a_F)}{\mp 2\pi m(1-a_R)} = 1$$

Then as $\sin\theta \to 0$ $\quad a_F = a_R = a = 0$.

Numerical checks have been made to verify the analytical development. Using idealized aerodynamics, ($C_L = 2\pi \sin\alpha$, $C_D = 0$),

it has been verified that:

1. $C_P)_{Max}$ is bounded by the Betz Limit for any pitch angle.
2. The Kutta-Joukowski term produces the only net power output.

CHAPTER 5

DARRIEUS ROTOR TEST DATA

In order to evaluate the accuracy of the theory developed in the previous sections, a comparison with test data is in order. The Sandia 17 meter and 5 meter machines offer the best source of test data taken over a range of operating conditions.

Two methods of data presentation are used. Figure 5-1 on the next page illustrates a power coefficient versus tip-speed ratio plot at various rpm. In this type of presentation, the low-wind-speed operating characteristics are easily illustrated. Maximum C_p and the effect of rpm (Reynolds number) are easily seen. The data used to plot Figure 5-1 came from Sandia 17 Meter test data. The geometry and physical characteristics are given in Appendix C.

Motoring of a rotor at low wind speed yields power requirements as $X \to \infty$. Such information can be used to determine the drag data. As shown in Chapter 2, the pitching terms do not contribute any net power when there is no induced velocity. Hence the motoring power input can be used to determine drag. Appendix D gives the calculation details. The results indicate that at 38.7 rpm $C_{D_0} = 0.00342$ and at 42.2 rpm, $C_{D_0} = 0.00705$. From Figure 5-1, it may be noted that the peak measured C_p is about 0.46 which is quite high. A C_p of 0.46 is also consistent with $C_{D_0} \simeq 0.00342$ which suggests a laminar boundary layer. The Eppler data for the NACA 0015 section, shown in Figure D-1, when

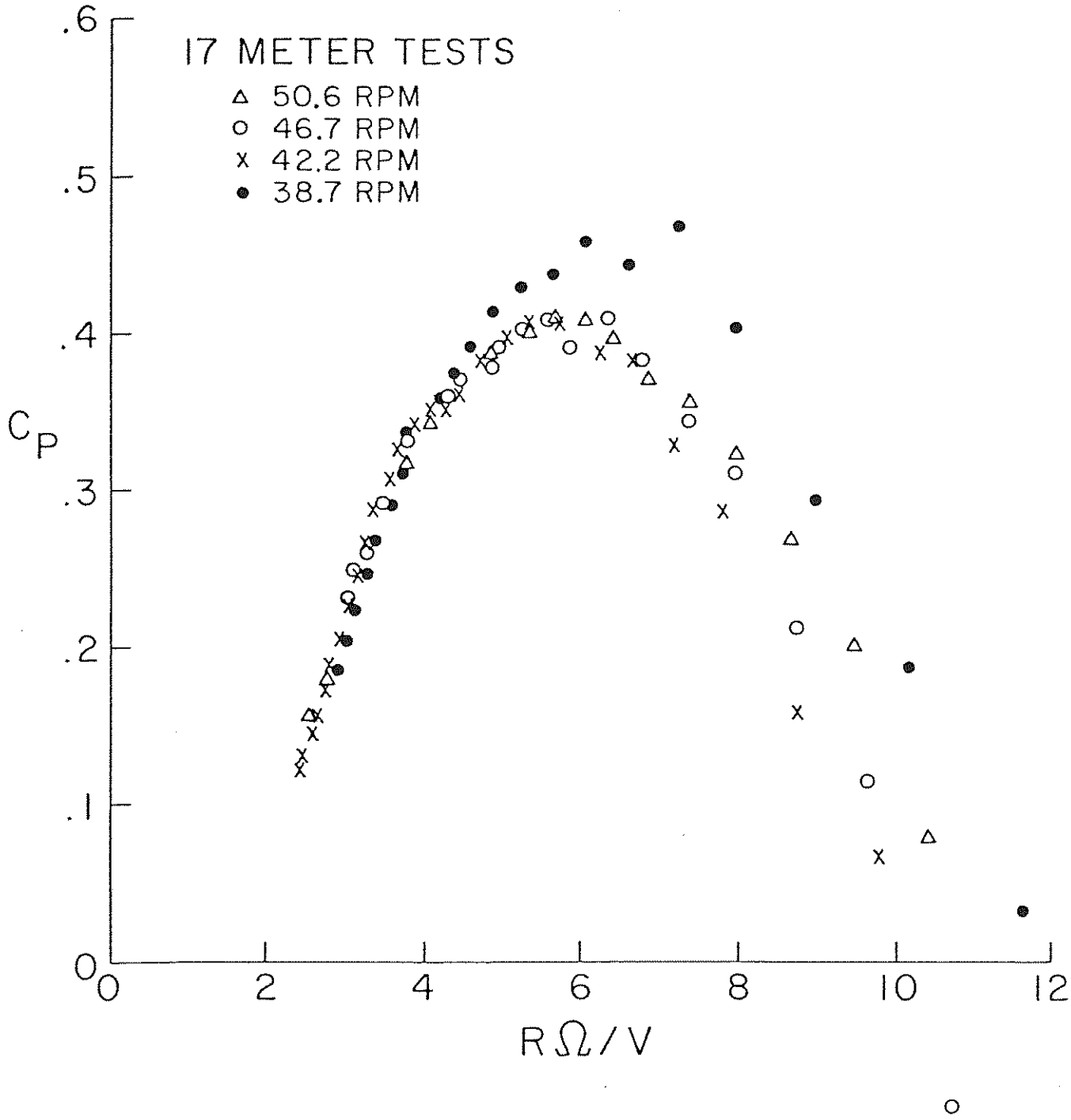

Figure 5-1 - Sandia 17 Meter Test Results. Each Data Point Represents At Least 1000 Samples.

compared to calculated values of C_{D_0} gives qualitative support to the idea that a laminar boundary layer exists up to $R_e \approx 10^6$.

While the C_p plot clearly illustrates the effects of flow variations at high tip speeds usual operation of Darrieus rotors is at constant rpm. Maximum rotor output at constant rpm occurs at low tip speed ratios where blade stall rather than C_{D_0} controls. Figure 5-2 is a plot of $K_p \equiv P/(\frac{1}{2}\rho(R\Omega)^3 A)$ versus $V/R\Omega$ for the 17 Meter machine. Here the rpm has a large effect on peak output. It has been suggested that dynamic stall controls peak machine output.

At low tip speed ratios (high wind speeds) most of the work is done by the advancing blade since the angle of attack is smaller when the relative wind is larger. The advancing blade also has a larger Reynolds number. In Appendix D, the Reynolds number range is plotted against $V/R\Omega$. These plots illustrate that the advancing blade Reynolds number varies considerably for the 17 Meter tests and supports the concept that dynamic stall may be the cause of the rpm effects.

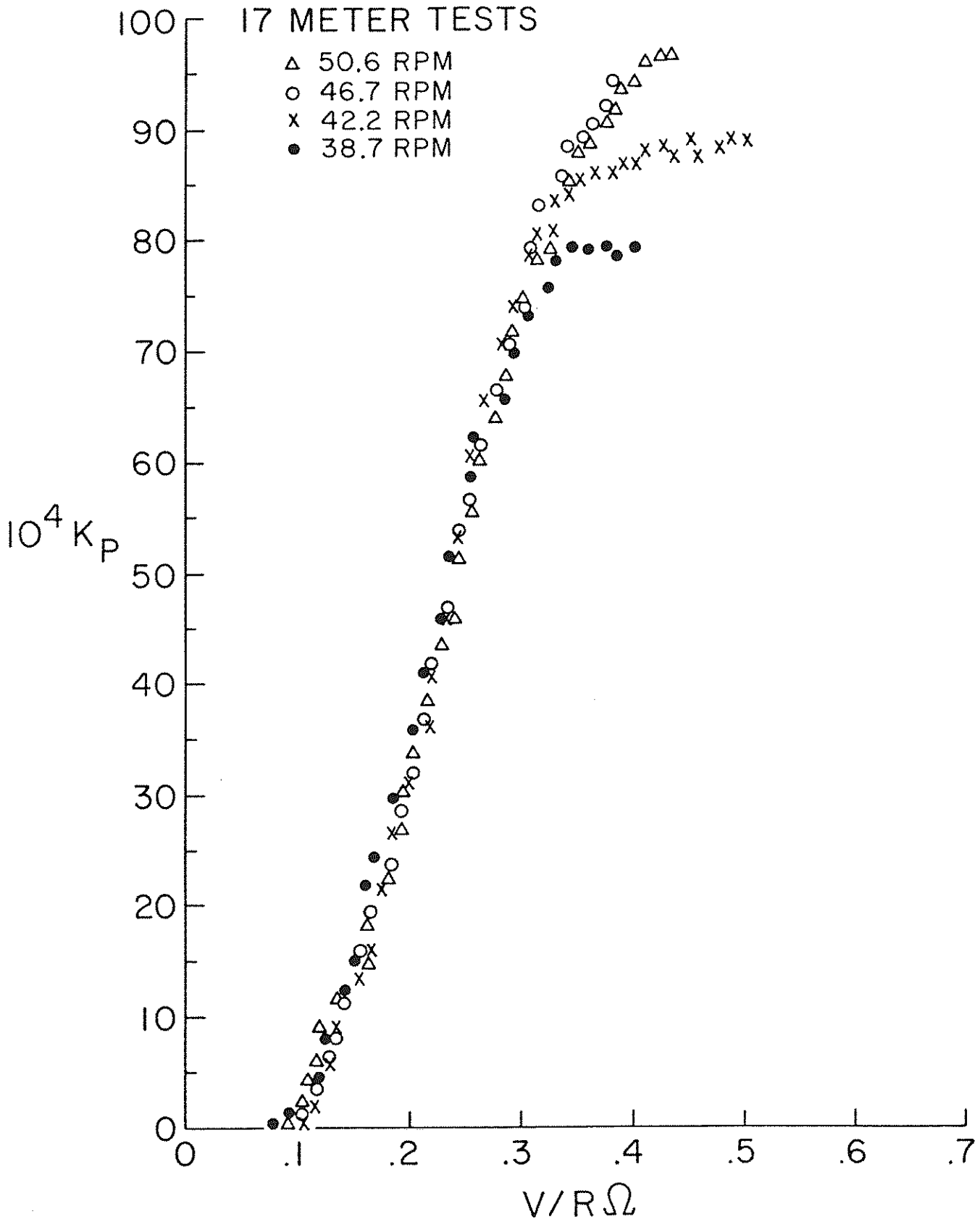

Figure 5-2 - Sandia 17 Meter Test Results. Each Data Point Reperesents At Least 100 Samples.

CHAPTER 6

ANALYTICAL RESULTS

The theory developed in the previous chapter has been compared with Sandia 17 m test data. Calculations were made using the Eppler tables suppled by Sandia for a NACA 0015 airfoil at a Reynolds number of 10^6. Figures 6-1 and 6-2 show the fixed wake theory. Table 6.1 below gives the test Reynolds number for each rpm.

Table 6.1. Test Reynolds Numbers.

RPM	$R_e \equiv R\Omega c/\nu$
38.7	$1.15 \cdot 10^6$
42.2	$1.25 \cdot 10^6$
46.7	$1.39 \cdot 10^6$
50.6	$1.50 \cdot 10^6$

In Figure 6-1, theoretical predictions are illustrated for the Eppler data which has $C_{D_0} = 0.0074$ and for the Eppler data modified to have $C_{D_0} = 0.0037$ which was the calculated value of C_{D_0} from motoring tests (see Appendix D). The predictions using the lower value of C_{D_0} agrees qualitatively with data, however, there is still far from perfect agreement. The variation of lift with Reynolds number was not considered nor

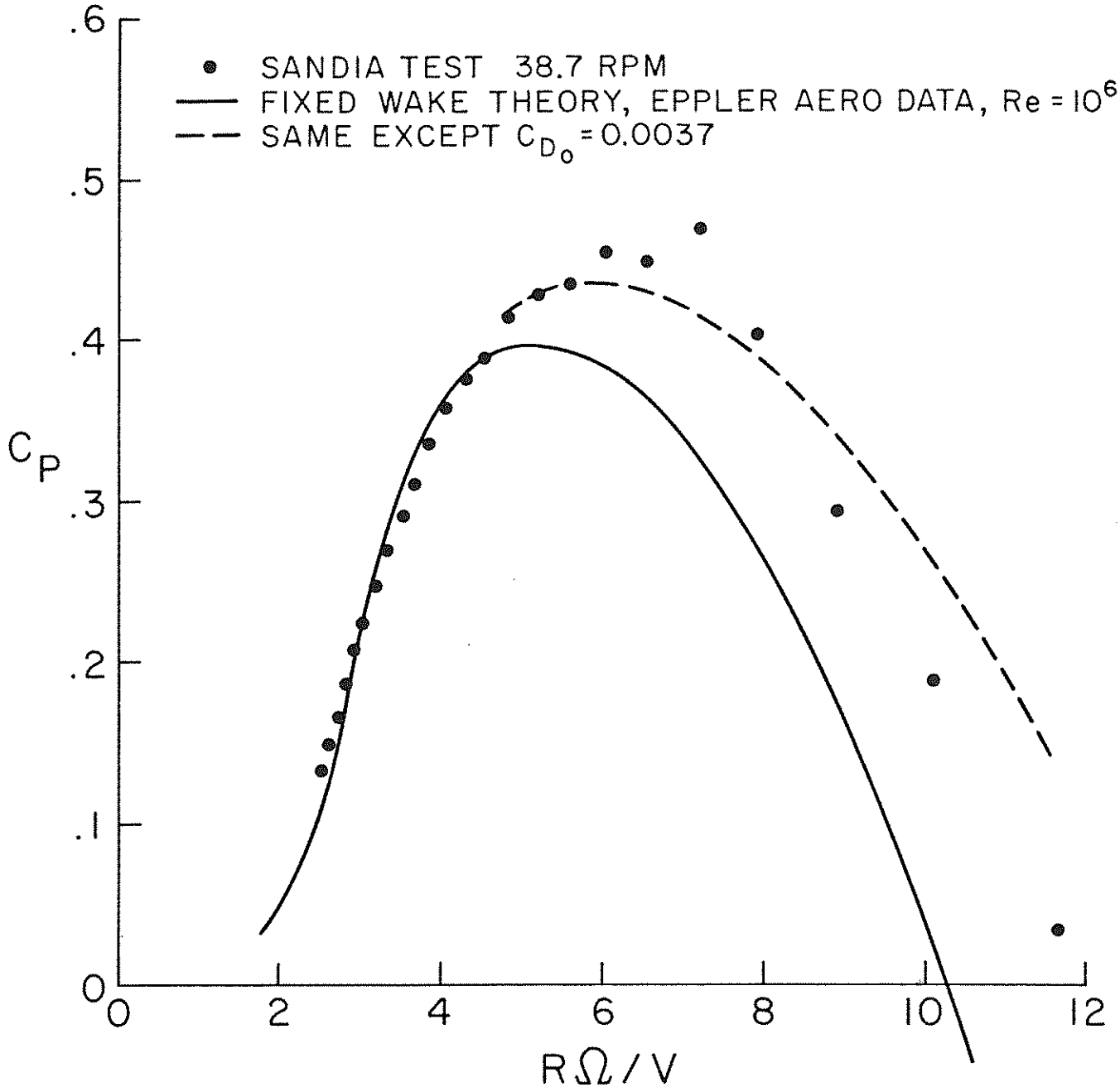

Figure 6-1 - Fixed Wake Theory and Test Results

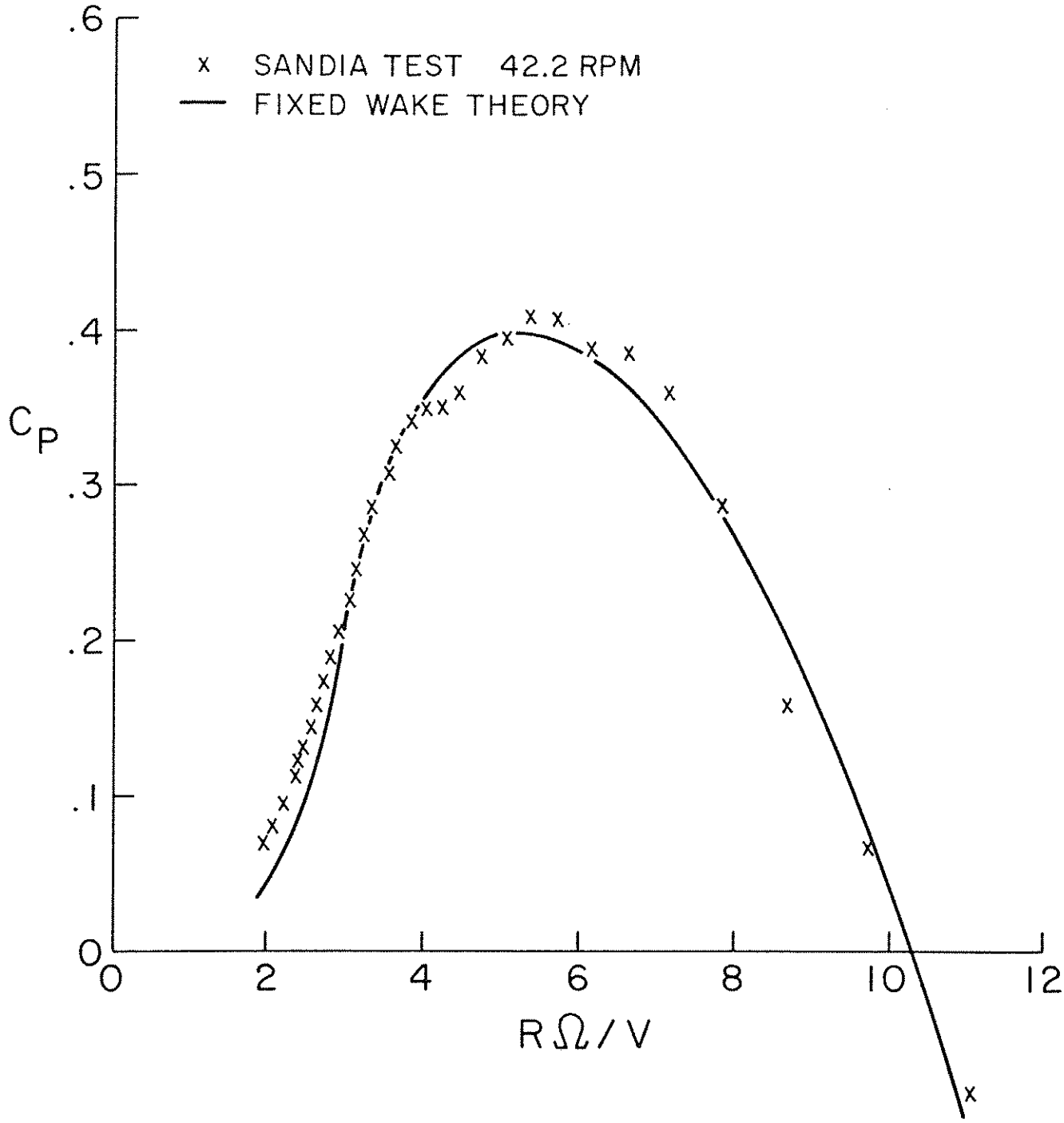

Figure 6-2 - Fixed Wake Theory and Test Results

were the local changes of C_D with Reynolds number. With a laminar boundary layer, such changes will be greater than in the case of a turbulent boundary layer.

Figure 6-2 illustrates the 42.2 rpm test data. In this case, the measured C_{D_0} is suggestive of a turbulent boundary layer and is in general agreement with the Eppler data ($C_{D_0} \approx .0071$). Agreement between theory and test results is good. At higher rpm as Figure 6-3 illustrates, the agreement is not as good as at 42.2 rpm. No data on C_{D_0} were available for 46.7 rpm or 50.6 rpm.

At low tip speed ratios, the agreement between theory and test is poor. Below a tip-speed ratio of 3, the 17 m test results show a significant rpm effect which has been thought to be due to dynamic stall. This effect was not included in the calculations.

The effects of blade pitch angle were examined numerically for this 17 m rotor geometry. Using Eppler airfoil data for $R_e = 10^6$ and $x_o = 0.38c$, rotor power coefficients were determined over a range of operating conditions. These results are shown in Figure 6-4(a) and 6-4(b). The results show an increased output for slightly positive pitch (leading edge out). The effect was greatest at X = 3 and greatly increased $K_p)_{Max}$. The type of blade pitch illustrated in Figure 6-4 corresponds to a rotation of this chord only. Sandia 5 m tests with blade pitch involve blade translation as well as rotation. Thus the 5 m test geometry is different than shown in Figure 6-4 and no comparison can be made.

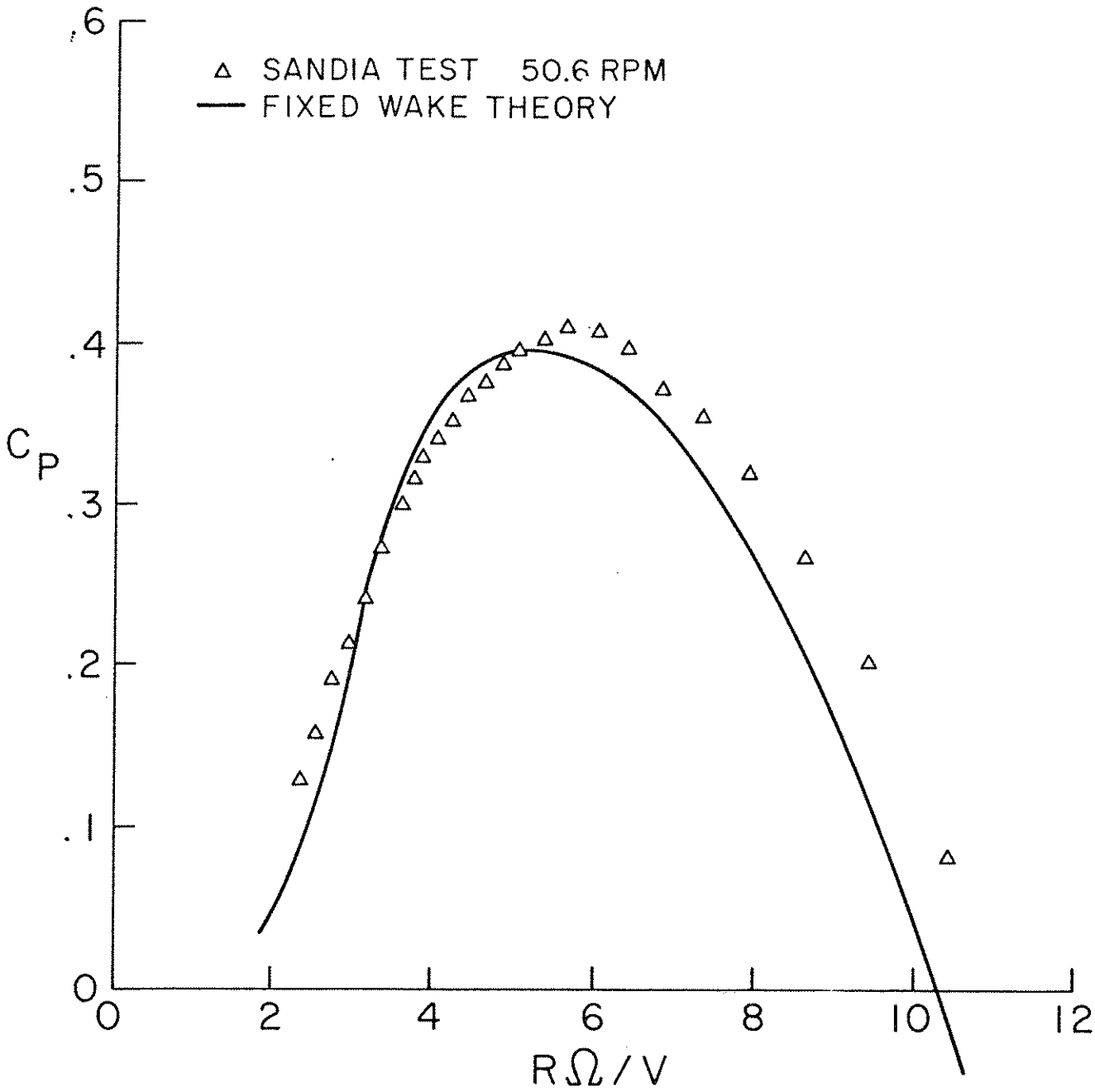

Figure 6-3 - Fixed Wake Theory and Test Results

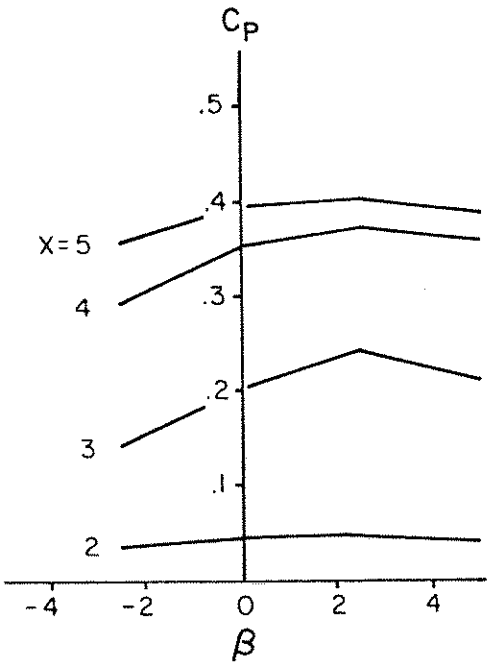

(a)

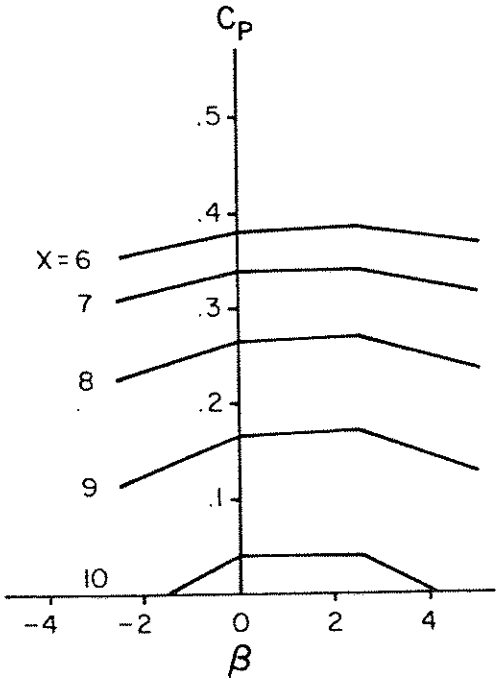

(b)

Figure 6-4 - Fixed Wake Predictions for Various Blade Pitch Angles

REFERENCES

1. Lissaman, P.B.S., R.E. Wilson and M. James, "Calculation of Forces and Moments on a Flat Plate in Non-Steady Flow," Oregon State University, Corvallis, Oregon, November 1978.

APPENDIX A

COMPUTER PROGRAM

```
      PROGRAM VAPP(TAPE3,INPUT,TAPE9,OUTPUT)
C
C
C     VERTICAL AXIS PERFORMANCE PROGRAM DEVELOPED BY STEL
C     N. WALKER AND ROBERT E. WILSON FOR SANDIA PERFORMANCE
C     STUDY - - FALL 1979
      DIMENSION ALI(150),CLI(150),CDI(150),CMI(150),TORQUE(150)
      COMMON ALI,CLI,CDI,CMI,N2,PI,AERO
C     INPUT PARAMETERS
C
C     ...NS = NUMBER OF HEIGHT STATIONS FOR EVALUATION
C     ...H = ROTOR HEIGHT / DIAMETER RATIO
C     ...B = NUMBER OF BLADES
C     ...ALI =AIRFOIL ANGLE OF ATTACK (DEGREES)
C     ...CLI =SECTIONAL LIFT COEFFICIENT
C     ...CDI = SECTIONAL DRAG COEFFICIENT
C     ...CMI = SECTIONAL MOMENT COEFFICIENT
C     ...N2 = NUMBER OF AIRFOIL PROPERTIES (DATA POINTS)
C     ...NCASE = NUMBER OF TIPSPEED RATIO CASES
C     ...XS = STARTING TIPSPEED RATIO FOR EVALUATION (>2)
C     ...GEOM = GEOMETRY SELECTOR, 1=PARABOLIC,2=CIRCULAR,3=STRAIGHT
C
C
C
C     READ INPUT
      PRINT 1
1     FORMAT(*ENTER,NS,H,B,CH,BETAH,Z1H*)
      READ *,NS,H,B,CH,BETAH,Z1H
      PRINT 2
2     FORMAT(*ENTER,XS,DXXX,NCASE,GEOM,AERO,N2*)
      READ *,XS,DXXX,NCASE,GEOM,AERO,N2
      PRINT 12,NS,H,B,CH,BETAH,Z1H
      PRINT 13,XS,DXXX,NCASE,GEOM,AERO,N2
13     FORMAT(F10.2,F10.2,3X,I3,2F10.4,3X,I5)
12    FORMAT(I3,5X,5F10.4)
      IF(AERO.LT.2.) GO TO 283
      DO 38 JLL=1,N2
      READ(3,23) ALI(JLL),CLI(JLL),CDI(JLL),CMI(JLL)

23    FORMAT(4F10.2)
38    CONTINUE
      PRINT14,ALI(1),CLI(1),CDI(1)
14    FORMAT(3F10.4)
283   CONTINUE
C
C
C
C
C     INITIALIZATION

C
      PI=3.14159265
      RM=1.
      PI2=PI/2.
      CONVT=PI/180.
      DZ=H/FLOAT(NS)
      X=XS
      RX=1./XS
C
C
C
      DO 5 LL=1,NCASE
      AREA=0.
      ZH=DZ/2.
      A=0.1
      QT=0.
      QTKJ=0.
      QTZ1=0.
      QTAL=0.
      QTFW=0.
      QTMW=0.
      QTM=0.
      FINT=0.
      QD=0.
      QDT=0.
      AN=0.
      BOB=-1.
      POP=-1.
      AF=0.5*(1.-SQRT(1.-2.*A))
      AR=0.5*(1.+2.*A-SQRT(1.-2.*A))
C
```

```
C
      DO 4 K=1,NS
C
C
      CALL GEOMET(GEOM,H,RM,RR,GG,R,ZH,G)
      CALL BLADE(ZH,C,BETA,RR,B,GG,Z1,CH,BETAH,Z1H)
      CR=B*C
      GGD=GG*180./PI
      BETAD=BETA*180./PI
      WRITE(9,91) BETAD,GGD,RR,CR,X
91    FORMAT(/,X,≠BETA  = ≠,F7.2,10X,≠GG  = ≠,F7.2,10X,≠RR  = ≠,F7.3,10X
     1,≠CR  = ≠,F6.4,10X,≠X  = ≠,F5.3,///)
      WRITE(9,89)
89    FORMAT(//,X,≠TDEG≠,7X,≠A≠,7X,≠ALEF≠,6X,≠CLF≠,6X,≠CDF≠,7X,
     1≠AF≠,7X,≠ALER≠,6X,≠CLR≠,6X,≠CDR≠,7X,≠AR≠,8X,≠DQN≠,8X,≠DQF≠,
     28X,≠DQR≠,/)
      FORCE=0.
      Q=0.
      QKJ=0.
      QZ1=0.
      QAL=0.
      QFW=0.
      QMW=0.
      QM=0.
      T=0.
      QD=0.
      N=35
C
C
      CGG=COS(GG)
      DT=PI/FLOAT(N+1)
      NNN=N+2
      DO 3 I=1,NNN
C
C
      C28=1.0
      IF(ABS(T).LT..0001) C28=.5
      IF(ABS(T-PI).LT..0001) C28=.5
      CALL CALC(A,G,T,RR, X,AERO,BETA,CR,PI,DQ,DQF,DQF,DELTQ,GG
     1,BOB,POP,B,DQKJ,DQZ1,DQAL,DQFW,DQMW,DQM,Z1)
C
C
      Q=Q+DQ*C28/FLOAT(N+1)
      C7=C28/FLOAT(N+1)
      QKJ=QKJ+C7*DQKJ
      QZ1=QZ1+C7*DQZ1
      QAL=QAL+C7*DQAL
      QFW=QFW+C7*DQFW
      QMW=QMW+C7*DQMW
      QM=QM+C7*DQM
      QD=QD+DELTQ*C28/FLOAT(N+1)
      DF=A*(1.-A)*SIN(T)*4.*RR*PI
      FORCE=FORCE+DF*C28/FLOAT(N+1)
 3    T=T+DT
      QT=QT+Q*DZ
      QTKJ=QTKJ+QKJ*DZ
      QTZ1=QTZ1+QZ1*DZ
      QTAL=QTAL+QAL*DZ
      QTFW=QTFW+QFW*DZ
      QTMW=QTMW+QMW*DZ
      QTM=QTM+QM*DZ
      QDT=QDT+QD*DZ
      FINT=FINT+FORCE*DZ
      CPLOC=X*Q/(2.*RR)
      WRITE(9,142) CPLOC
142   FORMAT(/,100X,≠CPLOCAL  = ≠,F7.4)
      AREA=AREA+RR*DZ
 4    ZH=ZH+DZ
      CP=X*QT/(2.*AREA)
      RKJ=QTKJ/QT
      RZ1=QTZ1/QT
      RAL=QTAL/QT
      RFW=QTFW/QT
      RMW=QTMW/QT
      RMM=QTM/QT
      DELCP=X*QDT/(2.*AREA)
      RATIO=CP*(10./X)**3
      DRATIO=DELCP*(10./X)**3
      CT=FINT/(2.*AREA)
C
```

```
C       OUTPUT STATEMENT
C
        PRINT 220,RKJ,RZ1,RAL
        WRITE(9,220) RKJ,RZ1,RAL
        PRINT 221,RFW,RMW,RMM
        WRITE(9,221) RFW,RMW,RMM


        PRINT 10,CP,CT,AREA,RATIO,DRATIO,DELCP,X
10      FORMAT(7F10.4)
220     FORMAT(//≠ RKJ = ≠,F10.4,5X,≠RZ1 = ≠,F10.4,5X,≠RAL = ≠,F10.4)
221     FORMAT(/≠ RFW = ≠,F10.4,5X,≠RMW = ≠,F10.4,5X,≠RMM = ≠,F10.4)
        WRITE(9,169) CP,CT,AREA,RATIO,DRATIO,DELCP,X
169     FORMAT(///,X,≠CP = ≠,F7.4,5X,≠CT = ≠,F7.4,5X,≠AREA = ≠,F7.4,5X
       1,≠RATIO = ≠,F10.5,5X,≠DRATIO = ≠,F10.5,5X,≠DELCP = ≠,F7.5,5X,
       2≠X = ≠,F7.3)
        X=X+DXXX
        IF(X.LT.1.) GO TO 6
  5     CONTINUE
  6     STOP
C
C       FORMAT STATEMENTS
C
C
        END
C
```

```
      SUBROUTINE CALC(A,G,T,RR, X,AERO,BETA,CR,PI,DQ,DQF,DQR,DELTQ
     1,GG,BOB,POP,B,DQKJ,DQZ1,DQAL,DQFW,DQMW,CQM,Z1)
      ATEST=0.05
      CALL NACA(ATEST,CLTT,CDTT,CMTT)
      ABEST=0.
      CALL NACA(ABEST,CTTT,CDTTT,CMTTT)
      AS=(CLTT-CTTT)/ATEST
      PI2=PI/2.
      C=CR/B
      AFOLD=5.
      CGG=COS(GG)
      SGG=SIN(GG)
      CALL NACA(BETA,CLB,CDB,CMB)
      SB=SIN(BETA)
      CB=COS(BETA)
      ST=SIN(T)
      CT=COS(T)
      SNT=-ST
      XL=RR*X
      XL2=XL*XL
      GCT=G*CT
      VP=CGG*X*C*(.75-Z1)
      GB=X*AS*((BETA*RR)-(C*CGG*(.75-Z1)))
      BCRX=CR*X/(4.*PI)
      KK=100
      IF(ST.LE..01) KK=1
      DO 4 J=1,KK
      IF(ST.GE..01) GO TO 105
      A=0.
      VT=XL+(1.-A)*GCT
      WEF=VT
      ALF=ATAN(VP/VT)
      ALEF=ALF-BETA
      CALL NACA(ALEF,CLF,CDF,CMF)
      GAMT=WEF*CLF
      GAMF=GAMT+GB
      AF=A
      AR=A
      ALER=ALEF
      ALF=ALEF
      ALR=ALER
      WER=WEF
      CLR=CLF
      CDR=CDF
      CMR=CMF
      AN=0.
      ALN=0.
      CALL NACA(ALN,CLN,CDN,CMN)
      WEN=XL+GCT
      ALOF=0.
      ALOR=ALOF
      GO TO 32
105   CONTINUE
      UN=1.-AN
      UP=1.-A
      UF=1.-AF
      UR=1.-AR
      VTF=XL+UF*GCT
      VTR=XL+UR*GCT
      VTN=XL+UN*GCT
      VNN=CGG*UN*G*ST
      ALN=ATAN(VNN /VTN)
      WEN2=VTN*VTN+VNN*VNN
      WEN=SQRT(WEN2)
      VNF=CGG*(UF*G*ST)
```

```
      VNR=CGG*(UR*G*SNT)
      ALOF=ATAN(VNF/VTF)
      ALOR=ATAN(VNR/VTR)
      TOPF=VP+VNF*CB-VTF*SB
      BOTF=VTF*CB+VNF*SB
      ALF=ATAN(TOPF/BOTF)
      TOPR=VP+VNR*CB-VTR*SB
      BOTR=VTR*CB+VNR*SB
      ALR=ATAN(TOPR/BOTR)
      WEF=SQRT(VTF*VTF+VNF*VNF)
      WER=SQRT(VTR*VTR+VNR*VNR)
      CALL NACA(ALN,CLN,CDN,CMN)
      CALL NACA(ALF,CLF,CDF,CMF)
      CALL NACA(ALR,CLR,CDR,CMR)
      GAMFT=WEF*CLF
      GAMRT=WER*CLR
      GAMF=GAMFT+GB
      GAMR=GAMRT+GB
      A=(BCRX/2.)*((GAMF/UP)-(GAMR/UP))/(G*G)
      PBSL=CR*X*(AS/PI)*.5*ST*CGG
      IF(PBSL.LE..1) PBSL=.1
      PETER=SQRT(1./PBSL)
      PETER=PETER-.70710678
      PETER=PETER*PETER
      IF(A.GT..48) A=0.5-PETER
      IF(ABS(GAMF).LT..001) GO TO 33
      BOB=GAMR/GAMF
      AF=A/(1.-BOB)
      AR=AF+A
      GO TO 35
33    IF(ABS(GAMR).LT..001) GO TO 34
      POP=GAMF/GAMR
      AF=-A*POP/(1.-POP)
      AR=AF+A
      GO TO 35
34    A=AF=AR=0.
35    CONTINUE
      AN=CR*X*WEN*CLN/(PI*4.*G*G*(1.-AN))
      IF(ABS(AF-AFOLD).LT..0001) GO TO 100
      AFOLD=AF
32    CONTINUE
4     CONTINUE
100   CONTINUE
      IF(J.EQ.KK) GO TO 5
      GO TO 6
5     PRINT 23
      TDEG=T*180./PI
      PRINT 144,TDEG
144   FORMAT( F8.1)
6     CONTINUE
23    FORMAT(≠CONVERGENCE CRITERIA WAS NOT MET≠)
      SAF=SIN(ALOF)
      CAF=COS(ALOF)
      SAR=SIN(ALOR)
      CAR=COS(ALOR)
      SSF=SIN(ALOF-BETA)
      CCF=COS(ALOF-BETA)
      SSR=SIN(ALOR-BETA)
      CCR=COS(ALOR-BETA)
      WEF2=WEF*WEF
      WER2=WER*WER
```

```
      ZCX=Z1-.25
      ZXC=1.-4.*Z1
      ZXCW=(1.-2.*Z1)**2
      CQGP=2.*PI*CR*C*RR*X*(.75-Z1)*CGG
      CQGB=CR*X*RR*RR*CGG*CLB
      DQGBF=CQGB*(1.-AF)*ST
      DQGBR=-CQGB*(1.-AR)*ST
      DQGPF=-CQGP*(1.-AF)*ST
      DQGPR=CQGP*(1.-AR)*ST
      DQKJF=WEF2*CR*RR*(CLF*SAF-CDF*CAF)/CGG
      DQKJR=WER2*CR*RR*(CLR*SAR-CDR*CAR)/CGG
      DQKJF=DQKJF+DQGBF+DQGPF
      DQKJR=DQKJR+DQGBR+DQGPR
      DQZ1F=WEF2*CR*C*ZCX*(CLF*CCF+CDF*SSF)
      DQZ1R=WER2*CR*C*ZCX*(CLR*CCR+CDR*SSR)
      DQALF=WEF*CR*C*X*PI2*RR*ZXC*SSF
      DQALR=WER*CR*C*X*PI2*RR*ZXC*SSR
      DQFWF=CR*C*C*X*X*PI2*CGG*ZXCW*RR
      DQFWR=DQFWF
      DQMWF=-WEF*CR*C*C*X*(PI2/4.)*CDF*CGG
      DQMWR=-WER*CR*C*C*X*(PI2/4.)*CDR*CGG
      DQMF=WEF2*CR*C*CMF
      DQMR=WER2*CR*C*CMR


      DQF=DQKJF+DQZ1F+DQALF+DQFWF+DQMWF+DQMF
      DQR=DQKJR+DQZ1R+DQALR+DQFWR+DQMWR+DQMR
      DQN=WEN*CR*RR*((CLN*G*(1.-AN)*ST)-(CDN/CGG)*
     1(RR*X+G*(1.-AN)*CT))
      DQ=(DQF+DQR)/2.
      DQKJ=(DQKJF+DQKJR)/2.
      DQZ1=(DQZ1F+DQZ1R)/2.
      DQAL=(DQALF+DQALR)/2.
      DQFW=(DQFWF+DQFWR)/2.
      DQMW=(DQMWF+DQMWR)/2.
      DQM=(DQMF+DQMR)/2.

      DELTQ=DQ-DQN
      RDEG=180./PI
      ALEFD=ALF*RDEG
      ALERD=ALR*RDEG
      TDEG=T*RDEG
      WRITE(9,99) TDEG,A,ALEFD,CLF,CDF,AF,ALERD,CLR,CDR,AR,DQN,DQF,DQR
99    FORMAT(X,F4.0,3X,F7.4,3X,F7.2,3X,F6.3,3X,F6.3,3X,F7.4,3X,
     1F7.2,3X,F6.3,3X,F6.3,3X,F7.4,3X,F8.5,3X,F8.5,3X,F8.5)
      RETURN
      END
C
```

```
C
      SUBROUTINE BLADE(ZH,C,BETA,RR,B,GG,Z1,CH,BETAH,Z1H)
      C=CH
      PI=3.14159265
      CONVT=PI/180.
      BETAD=BETAH*CONVT
      Z1=Z1H
      BETA=BETAD
      RETURN
      END
      SUBROUTINE GEOMET(GEOM,H,RM,RR,GG,R,ZH,G)
      IF(ABS(GEOM-1.).LT..1) GO TO 10
      IF(ABS(GEOM-2.).LT..1) GO TO 20
      IF(ABS(GEOM-3.).LT..1) GO TO 40
      IF((ZH/RM).GE..54954) GO TO 50
      RR=.33714+SQRT(.43939-(ZH/RM)**2)
      GG=ATAN((ZH/RM)/(RR-.33714))
      GO TO 30
50    CONTINUE
      RR=1.52253-1.48256*(ZH/RM)
      GG=0.97739
      GO TO 30
40    RR=1.
      GG=0.
      GO TO 30
10    RR=1.-.9575*(ZH/H)**2
      GG=ATAN(1.915*ZH/H)
      GO TO 30
20    RR=SQRT(1.-(ZH/RM)**2)
      GG=ATAN((ZH/RM)/RR)
30    R=RR*RM
      G=1.
      RETURN
      END
C
C
C
C
      SUBROUTINE NACA(AL,CL,CD,CM)
      DIMENSION ALI(150),CLI(150),CDI(150),CMI(150)
      COMMON ALI,CLI,CDI,CMI,N2,PI,AERO
      IF(ABS(AERO-1.).LT..1) GO TO 100
      IF(ABS(AERO-2.).LT..1) GO TO 120
      GO TO 120
100   CL=2.*PI*SIN(AL)
      CD=0.00
      GO TO 50
120   CONTINUE
      A=AL*180./PI
      DO 10 J=1,N2
      IF(A.LE.ALI(1)) GO TO 40
      IF(A.LE.ALI(J)) GO TO 20
      IF(J.EQ.N2) GO TO 30
10    CONTINUE
20    J=J+1
      PER=(A-ALI(J-1))/(ALI(J-2)-ALI(J-1))
      CL=PER*(CLI(J-2)-CLI(J-1))+CLI(J-1)
      CD=PER*(CDI(J-2)-CDI(J-1))+CDI(J-1)
      CM=PER*(CMI(J-2)-CMI(J-1))+CMI(J-1)
      GO TO 50
30    CL=CLI(N2)


      CD=CDI(N2)
      CM=CMI(N2)
      GO TO 50
40    CL=CLI(1)
      CD=CDI(1)
      CM=CMI(1)
50    CONTINUE
      RETURN
      END
```

APPENDIX B

LINEAR AERODYNAMICS

The solution using linear aerodynamics can be obtained. From Chapter 3 we recall

$$a(1-a) = \frac{BcX}{4R}\left(\frac{C_{L_F}}{2\pi}\frac{W_{e_F}}{V_R} - \frac{C_{L_R}}{2\pi}\frac{W_{e_R}}{V_R}\right)$$

Using $C_L = 2\pi m \sin(\alpha_e-\beta) = 2\pi m(\sin\alpha_o+\Delta\alpha-\beta)$, we note $\Delta\alpha \simeq c/RX\cos\gamma(3/4-x_o/c)/(x_L+(1-a)\cos\theta)$ is small so that $\sin\Delta\alpha \simeq \Delta\alpha$, $\cos\Delta\alpha \simeq 1$. Thus

$$\frac{C_L}{2\pi m} = \begin{Bmatrix} \cos\beta\sin\alpha_o \\ \cos\beta\cos\alpha_o\Delta\alpha \\ \\ \sin\beta\sin\alpha_o\Delta\alpha \\ -\sin\beta\cos\alpha_o \end{Bmatrix}$$

now $\frac{W_e}{V_R}\cos\alpha_o = x_L+u\cos\theta$

and

$$\frac{W_e}{V_R}\sin\alpha_o = u\cos\gamma\sin\theta$$

Thus

$$\frac{C_{L_F}}{2\pi m}\frac{W_{e_F}}{V_R} = \begin{Bmatrix} u_F\cos\beta\cos\gamma\sin\theta \\ u_P\cos\beta \\ u_F\sin\beta\cos\gamma\sin\theta u_P/(x_L+u_F\cos\theta) \\ -(x_L+u_F\cos\theta)\sin\beta \end{Bmatrix}$$

and

$$-\frac{C_{L_R}}{2\pi m}\frac{W_{e_R}}{V_R} = \left\{\begin{array}{l} u_R\cos\beta\cos\gamma\sin\theta \\ -u_P\cos\beta \\ u_R\sin\beta\cos\gamma\sin\theta u_P/(x_L+u_R\cos\theta) \\ +(x_L+u_R\cos\theta)\sin\beta \end{array}\right\}$$

$$u_P = \frac{c}{R}\,X\left(\frac{3}{4} - \frac{x_o}{c}\right)\cos\gamma$$

Thus we obtain

$$(1-a)a = \frac{BcmX}{4R}\left\{\begin{array}{l} (u_F+u_R)\cos\beta\cos\gamma\sin\theta \\ u_P\sin\beta\cos\gamma\sin\theta\left(\dfrac{u_F}{x_L+u_F\cos\theta} + \dfrac{u_R}{x_L+u_R\cos\theta}\right) \\ (u_R-u_F)\cos\theta\sin\beta \end{array}\right\}$$

When $\beta = 0$, a simple solution is obtained.

$$a(1-a) = \frac{BcmX}{4R}\cos\gamma\sin\theta(2-a_R-a_F)$$

From Chapter 4 we find for this case

$$\frac{\Gamma'_R}{\Gamma'_F} = -\frac{1-a_R}{1-a_F}$$

We obtain

$$\frac{a_R}{a_F} = 2 + \frac{1-a_R}{1-a_F}$$

using $a_R - a_F = a$

$$a_F = \frac{1-\sqrt{1-2a}}{2}$$

$$a_R = \frac{1+2a-\sqrt{1-2a}}{2}$$

The equation for a becomes

$$a(1-a) = \frac{BcmX}{4R} \cos\gamma \sin\theta (1-a+\sqrt{1-2a})$$

setting $\frac{BcmX}{4R} \cos\gamma \sin\theta \equiv z_o$ we assume a value of a, calculate z_o, a_R and a_F. The table below gives the induced velocity field as a function of z_o.

Note that as $z_o \to 0.5$

$$a \simeq \frac{1}{2}\left(\frac{2}{z_o} - \frac{1}{2z_o}\right)$$

z_o	a	a_F	a_R
.0502	.10	.0528	.1528
.1016	.20	.1127	.3127
.1576	.30	.1838	.4838
.2292	.40	.2764	.6764
.2857	.45	.3419	.7919
.3467	.48	.4000	.8800
.3836	.49	.4293	.9193
.4132	.495	.4500	.9450
.5000	.50	.5000	1.0000

Since $z_o)_{Max} = 0.5$, the theory predicts

$$X_{Max} = \frac{2}{Bc/R} \frac{1}{m\cos\gamma}$$

which for 2 bladed machines is about $(c/R)^{-1}$

With blade pitch the equations become more difficult to deal with. First we return to the expression

$$\frac{a_R}{a_F} = 2 - \frac{\Gamma'_R}{\Gamma'_F}$$

where the ratio of circulation is needed.

For $\gamma = 0$

$$\frac{\Gamma'_R}{\Gamma'_R} \simeq - \frac{1-a_R}{1-a_F} \frac{\sin(\theta+\beta)}{\sin(\theta-\beta)}$$

The effects of pitch on power, however, cannot be determined analytically.

Power

For zero pitch and large number of blades ($u_p \to 0$) we can determine the power

$$dP = \Omega dQ = \frac{\Omega}{2}\rho V_R^2 R^2 \left(\frac{Bc}{R}\right)\left(\frac{r}{R}\right)\left(\frac{W_e}{V_R}\right)^2 \frac{C_L(\alpha_e)\sin\alpha_o}{\cos\gamma}\, dz$$

but as $u_p \to 0$, $\alpha_e \to \alpha_o$ so that

$$(\frac{W_e}{V_R})^2 \; C_L \sin\alpha_o \rightarrow (\frac{W_e}{V_R})^2 \; 2\pi m \; \sin^2\alpha_o = 2\pi m u^2 \cos^2\gamma \sin^2\theta$$

Thus, since $\theta_R = -\theta_F = \theta$

$$dP = \frac{\Omega}{2} \rho V_R^2 R^2 (\frac{Bc}{R}) 2\pi m (\frac{r}{R}) dz \; \cos\gamma \sin^2\theta (u_F^2 + u_R^2)$$

but

$$u_F^2 + u_R^2 = (1-a)[(1-a) + \sqrt{1-2a}]$$

and

$$a(1-a) = (\frac{Bc}{R}) \; \frac{Xm}{4} \cos\gamma \sin\theta (1-a+\sqrt{1-2a})$$

so that

$$dP = 4\pi(\frac{1}{2}\rho V_R^3 2r) \sin\theta a (1-a)^2 dz$$

Defining a local power coefficient

$$C_{P_L} \equiv \frac{dP}{\frac{1}{2}\rho V_R^3 2r dz}$$

$$C_{P_L} = 4\pi \sin\theta a (1-a)^2$$

The average power coeffificient $\bar{C}_{P_L} = \frac{1}{\pi}\int_o^\pi C_{P_L} d\theta$

So that

$$\bar{C}_{P_L} = 4 \int_o^\pi a(1-a)^2 \sin\theta d\theta$$

and since $dx = r\sin\theta d\theta$

$$\bar{C}_{P_L} = 4 \int_{-r}^{r} a(1-a)^2 d\left(\frac{x}{r}\right)$$

which is $4a(1-a)^2$ averaged over the diameter of the turbine.

APPENDIX C

GEOMETRY

The blade geometry is shown below.

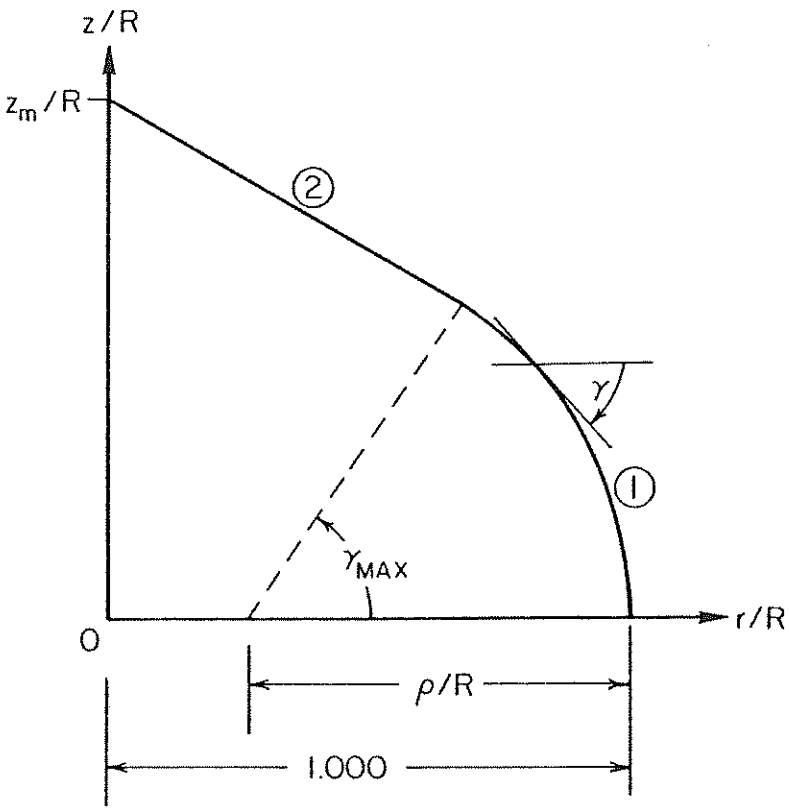

Figure C-1 - Rotor Blade Geometry

Region 1. $r/R = (1-\rho/R) + \sqrt{(\rho/R)^2-(z/R)^2}$

$\cos\gamma = \sqrt{1-(z/\rho)^2}$

Region 2. $r/R = C_1 - C_2(z/R)$

Machine	17 m	5 m
Blades	NACA 0015	NACA 0015
Chord	24"	6"
R_{Max}	325.86"	91.875"
c/R	0.07365	0.065371
B	2	2
x_o/c	0.38	0.41
ρ/R	.66286	.67597
z_{Max}/R	.97741	1.00265
γ_{Max}	56°	57.07°

$$\int_0^{z_{Max}} \frac{(r/R)^3 d(z/R)}{\cos\gamma} \approx 0.5607$$

$$\int_0^{z_{Max}} \frac{(r/R)^{5/2} d(z/R)}{\cos\gamma} \approx 0.6090$$

Area	$0.669\ R_{Max}^2$	$0.666\ R_{Max}^2$
C_1	1.52253	1.548036
C_2	1.48256	1.543944

APPENDIX D

DRAG COEFFICIENT

For very low wind speeds

$$dQ \rightarrow -\frac{1}{2}\rho r^3 \Omega^3 Bc C_{D_0} ds \qquad , \; ds = \frac{dz}{\cos\gamma}$$

$$dP = \Omega dQ = -\frac{1}{2}\rho\Omega^3 Bc \; C_{D_0} \frac{r^3 dz}{\cos\gamma}$$

$$P = -\frac{1}{2}\rho(R\Omega)^3 (\frac{Bc}{R}) R^2 \int_{-z_M}^{z_M} \frac{C_{D_0} (\frac{r}{R})^3}{\cos\gamma} d(\frac{z}{R})$$

For constant C_{D_0}

$$P = -\rho(R\Omega)^3 (\frac{Bc}{R}) R^2 C_{D_0} \; I_1$$

where

$$I_1 = \int_0^{z_M} \frac{(\frac{r}{R})^3}{\cos\gamma} d(\frac{z}{R})$$

For 17 m machine shape, $I_1 = 0.5607$ with $B = 2$ and $\rho = 0.001943$ slugs/ft^3

$$C_{D_0} = \frac{2.948 \cdot 10^8 (-kW)}{(RPM)^3 R^4 c}$$

where Ω is expressed in rpm and the input power is in kilowatts. For the 17 m rotor, $R = 27.155'$, $c = 2'$, so

$$C_{D_0} = \frac{271.08(-kW)}{(rpm)^3}$$

at 42.2 rpm, P = -1.9556 kW at V = 0.5 mph. The resulting C_{D_0} = 0.00705.

At 38.7 rpm, the power is -0.7953 kW which suggests a laminar boundary layer. Rather than using a constant C_{D_0}, let us use $C_{D_0} = KR_e^{-1/2}$ so

$$P = -\rho(R\Omega)^3\left(\frac{Bc}{R}\right)R^2 \sqrt{\frac{K}{R_{e_{Max}}}}\, I_2$$

where

$$I_2 = \int_0^{z_M} \frac{(r/R)^{5/2}}{\cos\gamma}\, d(z/R_M), \quad \sqrt{\frac{K}{R_{e_{Max}}}} = C_{D_0})_{Min}$$

For the 17 m shape, I_2 = 0.6090 so

$$C_{D_{0_{Min}}} = \frac{2.714\cdot 10^8(-kW)}{(rpm)^3 R^4 c} = \frac{249.59(-kW)}{(rpm)^3}$$

and for the 17 m

$$C_{D_{0_{Min}}} = 0.003425 \ (0.003720 \text{ using constant } C_D)$$

This corresponds to (since $R_e = 1.150\cdot 10^6$)

$$C_{D_0} = \frac{3.673}{\sqrt{R_e}}$$

For the 5 m symmetrical blade case R = 7.656', c = 6.003", B = 2 so that using 175 rpm results, P = -.229 kW and ($R_e = 3.665 \cdot 10^5$)

$$C_{D_{0_{Min}}} = 0.006751 = \frac{4.087}{\sqrt{R_e}}$$

The various values of C_{D_0} are plotted in Figure D-1. While three points are far from a convincing argument, there appears a possibility that transition for the symmetrical blades at low wind speeds is in the range $1.15 \cdot 10^6$ to $1.25 \cdot 10^6$.

Figures D-2 and D-3 illustrate Reynolds number variations for the test runs.

Going back to the 17 m test results, there is a question of whether the magnitude of measured difference in C_p between the 38.7 rpm and the 42.2 rpm runs is consistent with this measured differences in C_{D_0}. Using a constant C_{D_0} for each case the previously developed expression becomes

$$\Delta C_p = 0.419\left(\frac{Bc}{R}\right)X^3 \Delta C_{D_0}$$

the values of $\frac{Bc}{R} = 0.1473$ and $\Delta C_{D_0} = 0.00333$ yield

$$\Delta C_p = X^3/4866$$

Using linear interpolation from test data, the ΔC_p's are:

X	$\Delta C_p = C_{p_{38.7\ rpm}} - C_{p_{42.2\ rpm}}$
6.0	.065
6.5	.067
7.0	.100
7.5	.130
8.0	.130
8.5	.145
9.0	.150
9.5	.156
10.0	.165
10.5	.160
11.0	.180

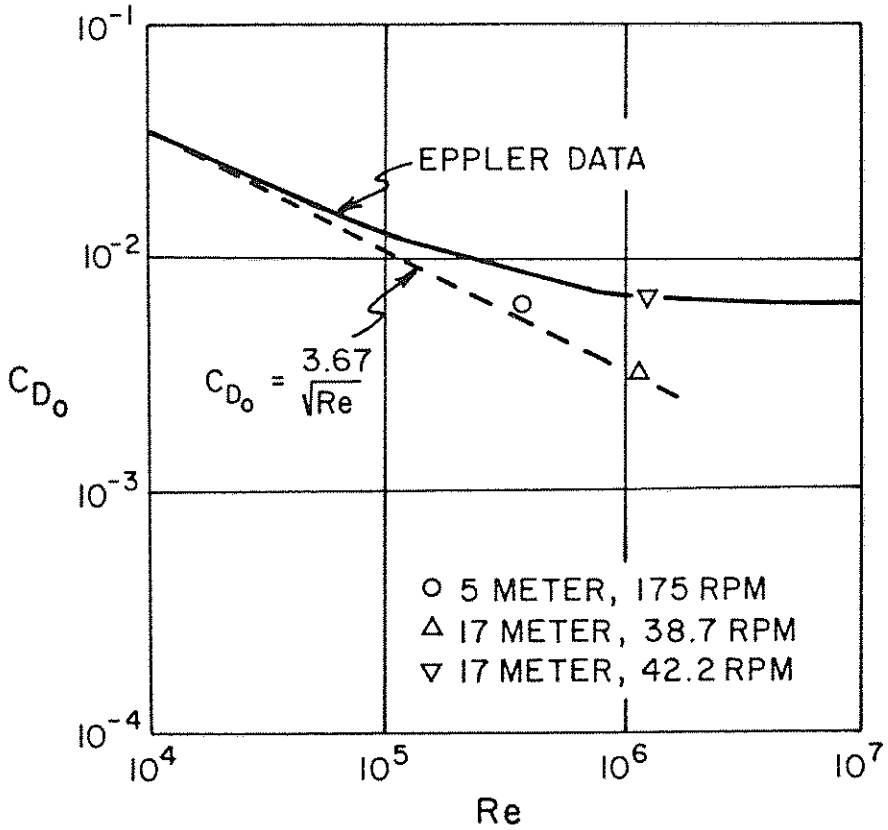

Figure D-1 - C_{D_0} versus Reynolds Number

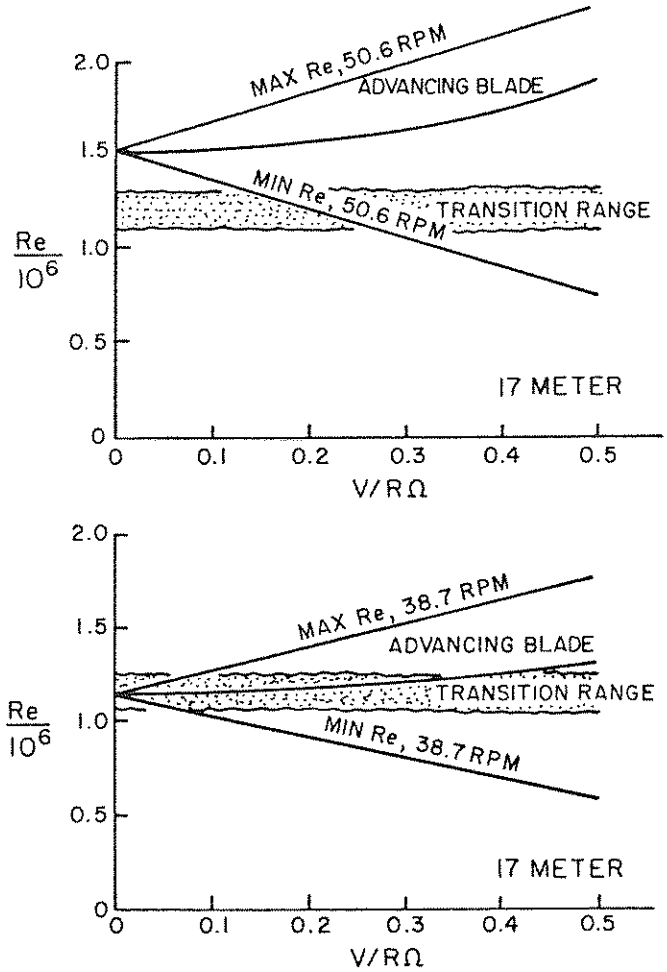

Figure D-2 - Reynolds Number Variation, 17 meter Machine

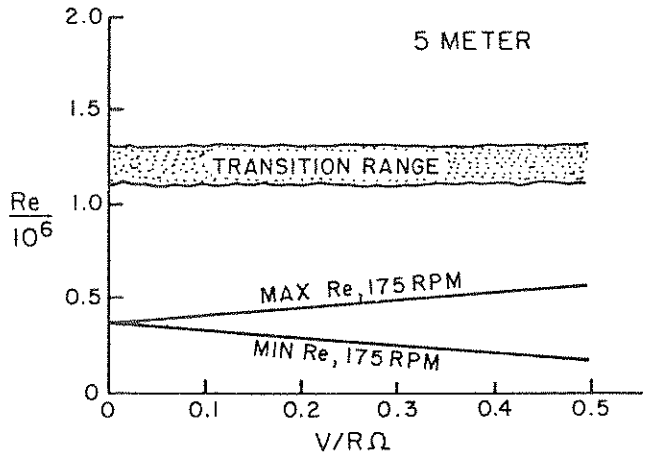

Figure D-3 - Reynolds Number Variation,
5 meter Machine

DISTRIBUTION:

TID-4500-R66 UC-60 (283)

Aero Engineering Department (2)
Wichita State University
Wichita, KS 67208
Attn: M. Snyder
W. Wentz

R. E. Akins, Assistant Professor
Department of Engineering Science
and Mechanics
Virginia Polytechnic Institute and
State University
Blacksburg, VA 24060

Alcoa Laboratories (5)
Alcoa Technical Center
Aluminum Company of America
Alcoa Center, PA 15069
Attn: D. K. Ai
A. G. Craig
J. T. Huang
J. R. Jombock
P. N. Vosburgh

Mr. Robert E. Allen
General Manager
Dynergy Corporation
P.O. Box 428
1269 Union Avenue
Laconia, NH 03246

American Wind Energy Association
1609 Connecticut Avenue NW
Washington, DC 20009

E. E. Anderson
South Dakota School of Mines
and Technology
Department of Mechanical Engineering
Rapid City, SD 57701

Scott Anderson
318 Millis Hall
University of Vermont
Burlington, VT 05405

G. T. Ankrum
DOE/Office of Commercialization
20 Massachusetts Avenue NW
Mail Station 2221C
Washington, DC 20585

Holt Ashley
Stanford University
Department of Aeronautics and
Astronautics Mechanical Engineering
Stanford, CA 94305

Kevin Austin
Consolidated Edison Company of
New York, Inc.
4 Irving Place
New York, NY 10003

B. H. Barksdale, Jr.
Hayes, Seay, Mattern, and Mattern
1315 Franklin Road SW
Roanoke, VA 24016

Dr. P. J. Baum
Institute of Geophysics
and Planetary Physics
University of California
Riverside, CA 92521

F. K. Bechtel
Washington State University
Department of Electrical Engineering
College of Engineering
Pullman, WA 99163

M. E. Beecher
Arizona State University
Solar Energy Collection
University Library
Tempe, AZ 85281

Leon Bjervig
Civilingenior, MCIF
"Osterbyhus", 6990 Ulfborg
DK6990
DENMARK

K. Bergey
University of Oklahoma
Aero Engineering Department
Norman, OK 73069

Steve Blake
Wind Energy Systems
Route 1, Box 93-A
Oskaloosa, KS 66066

Robert Brulle
McDonnell-Douglas Aircraft Corporation
P.O. Box 516
Department 341, Building 32/2
St. Louis, MO 63166

R. Camerero
Faculty of Applied Science
University of Sherbrooke
Sherbrooke, Quebec
CANADA J1K 2R1

CERCEM
49 Rue du Commandant Rolland
93350 Le Bourget
FRANCE
Attn: G. Darrieus
J. Delassus

Professor V. A. L. Chasteau
School of Engineering
University of Auckland
Private Bag
Auckland, NEW ZEALAND

Howard T. Clark
McDonnell Aircraft Corporation
P.O. Box 516
Department 337, Building 32
St. Louis, MO 63166

Dr. R. N. Clark
USDA, Agricultural Research Service
Southwest Great Plains Research Center
Bushland, TX 79012

Joan D. Cohen
Consumer Outreach Coordinator
State of New York
Executive Department
State Consumer Protection Board
99 Washington Avenue
Albany, NY 12210

Dr. D. E. Cromack
Associate Professor
Mechanical and Aerospace Engineering
Department
University of Massachusetts
Amherst, MA 01003

Gale B. Curtis
Tumac Industries
650 Ford Street
Colorado Springs, CO 80915

DOE/ALO (2)
Albuquerque, NM 87115
Attn: G. P. Tennyson

DOE Headquarters/WESD (20)
600 E Street NW
Washington, DC 20585
Attn: D. F. Ancona
C. E. Aspliden
L. V. Divone
W. C. Reddick

C. W. Dodd
School of Engineering
Southern Illinois University
Carbondale, IL 62901

D. D. Doerr
Kaiser Aluminum and Chemical Sales, Inc.
6177 Sunol Blvd.
P.O. Box 877
Pleasonton, CA 94566

Dominion Aluminum Fabricating Ltd. (2)
3570 Hawkestone Road
Mississauga, Ontario
CANADA L5C 2U8
Attn: L. Schienbein
C. Wood

D. P. Dougan
Hamilton Standard
1730 NASA Boulevard
Room 207
Houston, TX 77058

J. B. Dragt
Nederlands Energy Research Foundation (E.C.N.)
Physics Department
Westerduinweg 3 Patten (nh)
THE NETHERLANDS

C. E. Elderkin
Battelle-Pacific Northwest Laboratory
P.O. Box 999
Richland, WA 99352

Frank R. Eldridge, Jr.
The Mitre Corporation
1820 Dolley Madison Blvd.
McLean, VA 22102

Electric Power Research Institute
3412 Hillview Avenue
Palo Alto, CA 94304
Attn: E. Demeo

Richard G. Ferreira, Chief
The Resources Agency
Department of Water Resources
Energy Division
1416 9th Street
P.O. Box 388
Sacremento, CA 95802

D. R. Finley
New England Geosystems
P.O. Box 128
East Derry, NH 03041

James D. Fock, Jr.
Department of Aerospace Engineering Sciences
University of Colorado
Boulder, CO 80309

Dr. Lawrence C. Frederick
Public Service Company of New Hampshire
1000 Elm Street
Manchester, NH 03105

H. Gerardin
Mechanical Engineering Department
Faculty of Sciences and Engineering
Universite Laval-Quebec
CANADA G1K 7P4

E. Gilmore
Amarillo College
Amarillo, TX 79100

Paul Gipe
Wind Power Digest
P.O. Box 539
Harrisburg, PA 17108

Roger T. Griffiths
University College of Swansea
Department of Mechanical Engineering
Singleton Park
Swansea SA2 8PP
UNITED KINGDOM

Professor G. Gregorek
Ohio State University
Aeronautical and Astronautical Department
2070 Neil Avenue
Columbus, OH 43210

Richard Haddad
101 Arizona
P.O. Box 530
El Paso, TX 79944

A. A. Hagman
Kaiser Aluminum and Chemical Sales, Inc.
14200 Cottage Grove Avenue
Dolton, IL 60419

Martin L. Hally, Section Manager
Project Department
Electricity Supply
18 St. Stephen's Green
Dublin 2, IRELAND

Professor N. D. Ham
Massachusetts Institute of Technology
77 Massachusetts Avenue
Cambridge, MA 02139

C. F. Harris
Wind Engineering Corporation
Airport Industrial Area
Box 5936
Lubbock, TX 79415

W. L. Harris
Aero/Astro Department
Massachusetts Institute of Technology
Cambridge, MA 02139

Terry Healy (2)
Rockwell International
Rocky Flats Plant
P.O. Box 464
Golden, CO 80401

Helion
P.O. Box 4301
Sylmar, CA 91342

Don Hinrichsen
Associate Editor
AMBIO
KVA
Fack, S-10405
Stockholm
SWEDEN

Sven Hugosson
Box 21048
S. 100 31 Stockholm 21
SWEDEN

O. Igra
Department of Mechanical Engineering
Ben-Gurion University of the Negev
Beer-Sheva, ISRAEL

Indian Oil Corporation, Ltd.
Marketing Division
254-C, Dr. Annie Besant Road
Prabhadevi, Bombay-400025
INDIA

JBF Scientific Corporation
2 Jewel Drive
Wilmington, MA 01887
Attn: E. E. Johanson

Dr. Gary L. Johnson, P.E.
Electrical Engineering Department
Kansas State University
Manhattan, KS 66506

B. O. Kaddy, Jr.
Box 353
31 Union Street
Hillsboro, NH 03244

Kaman Aerospace Corporation
Old Windsor Road
Bloomfield, CT 06002
Attn: W. Batesol

F. L. Katzenberg
2820 Upton St. NW
Washington, DC 20008

Robert E. Kelland
The College of Trades and Technology
P.O. Box 1693
Prince Philip Drive
St. John's, Newfoundland
CANADA A1C 5P7

S. King
Natural Power, Inc.
New Boston, NH 03070

Larry Kinnett
P.O. Box 6593
Santa Barbara, CA 93111

Richard H. Klein
KW Control Systms, Inc.
27727 Conestoga Dr.
Rolling Hills Estates, CA 90274

Samuel H. Kohler
272 Old Delp Road
Lancaster, PA 17602

O. Krauss
Michigan State University
Division of Engineering Research
East Lansing, MI 48824

Carol Lamb
2584 East Geddes Avenue
Littleton, CO 80122

Lawrence Livermore Laboratory
P.O. Box 808 L-340
Livermore, CA 94550
Attn: D. W. Dorn

M. Lechner
Public Service Company of New Mexico
P.O. Box 2267
Albuquerque, NM 87103

Kalman Nagy Lehoczky
Cort Adelers GT. 30
Oslo 2
NORWAY

George E. Lennox
Industry Director
Mill Products Division
Reynolds Metals Company
6601 West Broad Street
Richmond, VA 23261

J. Lerner
State Energy Commission
Research and Development Division
1111 Howe Avenue
Sacramento, CA 95825

L. Liljidahl
Building 303
Agriculture Research Center
USDA
Beltsville, MD 20705

P. B. S. Lissaman
Aeroenvironment, Inc.
660 South Arroyo Parkway
Pasadena, CA 91105

Olle Ljungstrom
FFA, The Aeronautical Research Institute
Box 11021
S-16111 Bromma
SWEDEN

T. H. Logan
U.S. Turbine Corporation
Olde Courthouse Building
Canfield, OH 44406

J. B. Longendyck
Siltex
7 Capitol Drive
Moonachie, NJ 07074

Los Alamos Scientific Laboratories
P.O. Box 1663
Los Alamos, NM 87544
Attn: J. D. Balcomb Q-DO-T

Beatrice de Saint Louvent
Establissement d'Etudes et de Recherches
Meteorologigues
77, Rue de Serves
92106 Boulogne-Billancourt Cedex
FRANCE

Ernel L. Luther
Senior Associate
PRC Energy Analysis Co.
7600 Old Springhouse Rd.
McLean, VA 22101

L. H. J. Maile
48 York Mills Rd.
Willowdale, Ontario
CANADA M2P 1B4

E. L. Markowski
Motolola, Inc.
G.E.D.
Mail Drop 1429
8201 E. McDowell Rd.
P.O. Box 1417
Scottsdale, AZ 85252

Jacques R. Maroni
Ford Motor Company
Environmental Research and Energy
Planning Director
Environmental and Safety Engineering Staff
The American Road
Dearborn, MI 48121

Frank Matanzo
Dardalen Associates
15110 Frederick Road
Woodbine, MD 21797

H. S. Matsuda, Manager
Composite Materials Laboratory
Pioneering R&D Laboratories
Toray Industries, Inc.
Sonoyama, Otsu, Shiga
JAPAN 520

J. R. McConnell
Tumac Industries, Inc.
650 Ford St.
Colorado Springs, CO 80915

James Meiggs
Kaman Sciences Corporation
P.O. Box 7463
Colorado Springs, CO 80933

R. N. Meroney
Colorado State University
Department of Civil Engineering
Fort Collins, CO 80521

G. N. Monsson
Department of Economic Planning
and Development
Barrett Building
Cheyenne, WY 82002

Napier College of Commerce and Technology
Tutor Librarian, Technology Faculty
Colinton Road
Edinburgh, EH10 5DT
ENGLAND

NASA Lewis Research Center (4)
21000 Brookpark Road
Cleveland, OH 44135
Attn: J. Savino
R. L. Thomas
W. Robbins
K. Kaza

Anthony A. Nedd
The Power Company, Inc.
P.O. Box 221
Genesee Depot, WI 53217

V. Nelson
West Texas State University
Department of Physics
P.O. Box 248
Canyon, TX 79016

Leander Nichols
Natural Power, Inc.
New Boston, NH 03070

Ronald Nousain
P.O. Box 111
Rome 1132
Los Angeles, CA 90051

Roger O'Hara
Energy Times
909 NE 43rd
Suite 308
Seattle, WA 98105

Oklahoma State University (2)
Stillwater, OK 76074
Attn: W. L. Hughes
EE Department
D. K. McLaughlin
ME Department

Oregon State University (2)
Corvallis, OR 97331
Attn: R. E. Wilson
ME Department
R. W. Thresher
ME Department

Pat F. O'Rourke
Precinct 4
County Commissioner
City-County Building
El Paso, TX 79901

H. H. Paalman
Dow Chemical USA
Research Center
2800 Mitchell Drive
Walnut Creek, CA 94598

Dr. Y. H. Pao, Chairman
Flow Industries, Inc.
21414 68th Ave. South
Kent, WA 98031

Ion Paraschivoiu
IREQ
1800 montee Ste-Julie
Varennes, Qeubec
CANADA JOL 2PO

R. A. Parmalee
Northwestern University
Department of Civil Engineering
Evanston, IL 60201

Helge Petersen
Riso National Laboratory
DK-4000 Roskilde
DENMARK

Wilson Prichett, III
National Rural Electric Cooperative
  Association
1800 Massachusetts Avenue NW
Washington, DC 20036

Dr. Barry Rawlings, Chief
Division of Mechanical Engineering
Commonwealth Scientific and Industrial
  Research Organization
Graham Road, Highett
Victoria, 3190
AUSTRALIA

Thomas W. Reddoch
Associate Professor
Department of Electrical Engineering
The University of Tennessee
Knoxville, TN 37916

Ray G. Richards
Atlantic Wind Test Site
P.O. Box 189
Tignish P.E.I.
COB 2BO CANADA

A. Robb
Memorial University of Newfoundland
Faculty of Engineering and Applied Sciences
St. John's Newfoundland
CANADA A1C 5S7

J. R. Rodriguez
Solarwind Energy Corporation
1163 Pomona Road
Unit A
Corona, CA 91720

Dr. -Ing. Hans Ruscheweyh
Institut fur Leichbau
Technische Hochschule Aachen
Wullnerstrasse 7
GERMANY

Gwen Schreiner
Librarian
National Atomic Museum
Albuquerque, NM 87185

Douglas B. Seely, P.E.
U.S. Department of Energy
P.O. Box 3621
102 NE Holladay
Portland, OR 97208

Arnan Seginer
Professor of Aerodynamics
Technion-Israel Institute of
Technology
Department of Aeronautical
Engineering
Haifa, ISRAEL

Dr. Horst Selzer
Dipl.-Phys.
Wehrtechnik und Energieforschung
ERNO-Raumfahrttechnik GmbH
Hunefeldstr. 1-5
Postfach 10 59 09
2800 Bremen 1
GERMANY

H. Sevier
Rocket and Space Division
Bristol Aerospace Ltd.
P.O. Box 874
Winnipeg, Manitoba
CANADA R3C 2S4

P. N. Shankar
Aerodynamics Division
National Aeronautical Laboratory
Bangalore 560017
INDIA

David Sharpe
Kingston Polytechnic
Canbury Park Road
Kingston, Surrey
UNITED KINGDOM

D. G. Shepherd
Cornell University
Sibley School of Mechanical and
Aerospace Engineering
Ithaca, NY 14853

Dr. Fred Smith
Mechanical Engineering Department Head
Colorado State University
Ft. Collins, CO 80521

Kent Smith
Instituto Technologico Costa Rica
Apartado 159 Cartago
COSTA RICA

Leo H. Soderholm
Iowa State University
Agricultural Engineering, Room 213
Ames, IA 50010

Bent Sorenson
Roskilde University Centery
Energy JGroup, Bldg. 17.2
IMFUFA
P.O. Box 260
DK-400 Roskilde
DENMARK

Southwest Research Institute (2)
P.O. Drawer 28501
San Antonio, TX 78284
Attn: W. L. Donaldson, Senior Vice President
R. K. Swanson

Rick Stevenson
Route 2
Box 85
Springfield, MO 65802

Dale T. Stjernholm, P.E.
Mechanical Design Engineer
Morey/Stjernholm and Associates
1050 Magnolia Street
Colorado Springs, CO 80907

G. W. Stricker
130 Merchant St. #1104
Honolulu, HI 96813

C. J. Swet
Route 4
Box 358
Mt. Airy, MD 21771

John Taylor
National Research Council
ASEB
2101 Constitution Avenue
Washington, DC 20418

R. J. Templin (3)
Low Speed Aerodynamics Section
NRC-National Aeronautical Establishment
Ottawa 7, Ontario
CANADA K1A OR6

Texas Tech University (3)
P.O. Box 4389
Lubbock, TX 79409
Attn: K. C. Mehta, CE Department
J. Strickland, ME Department
J. Lawrence, ME Department

Fred Thompson
Atari, Inc.
155 Moffett Park Drive
Sunnyvale, CA 94086

J. M. Turner, Group Leader
Terrestrial Energy Technology Program Office
Energy Conversion Branch
Aerospace Power Division
Aero Propulsion Laboratory
Department of the Air Force
Air Force Wright Aeronautical Laboratories (AFSC)
Wright-Patterson Air Force Base, OH 45433

United Engineers and Constructors, Inc.
Advanced Engineering Department
30 South 17th Street
Philadelphia, PA 19101
Attn: A. J. Karalis

University of New Mexico (2)
New Mexico Engineering Research Institute
Campus, P.O. Box 25
Albuquerque, N.M. 87131
Attn: G. G. Leigh

University of New Mexico (2)
Albuquerque, NM 87106
Attn: K. T. Feldman
Energy Research Center
V. Sloglund
ME Department

Jan Vacek
Eolienne experimentale
C.P. 279, Cap-aux-Meules
Iles de la Madeleine, Quebec
CANADA

Irwin E. Vas
Solar Energy Research Institute
1617 Cole Blvd.
Golden, CO 80401

Otto de Vries
National Aerospace Laboratory
Anthony Fokkerweg 2
Amsterdam 1017
THE NETHERLANDS

R. Walters
West Virginia University
Department of Aero Engineering
1062 Kountz Avenue
Morgantown, WV 26505

E. J. Warchol
Bonneville Power Administration
P.O. Box 3621
Portland, OR 97225

D. F. Warne, Manager
Energy and Power Systems
ERA Ltd.
Cleeve Rd.
Leatherhead
Surrey KT22 7SA
ENGLAND

G. R. Watson, Project Manager
The Energy Center
Pennine House
4 Osborne Terrace
Newcastle upon Tyne NE2 1NE
UNITED KINGDOM

R. J. Watson
Watson Bowman Associates, Inc.
1280 Niagara St.
Buffalo, NY 14213

R. G. Watts
Tulane University
Department of Mechanical Engineering
New Orleans, LA 70018

W. G. Wells, P.E.
Associate Professor
Mechanical Engineering Department
Mississippi State University
Mississippi State, MS 39762

T. Wentink, Jr.
University of Alaska
Geophysical Institute
Fairbanks, AK 99701

West Texas State University
Government Depository Library
Number 613
Canyon, TX 79015

Wind Energy Report
Box 14
102 S. Village Ave.
Rockville Centre, NY 11571
Attn: Farrell Smith Seiler

Wind Program Manager
Wisconsin Division of State Energy
8th Floor
101 South Webster Street
Madison, WI 53702

Richard E. Wong
Assistant Director
Central Solar Energy Research Corp.
1200 Sixth Street
328 Executive Plaza
Detroit, MI 48226

1000 G. A. Fowler
1200 L. D. Smith
2525 R. P. Clark
3141 T. L. Werner (5)
3151 W. L. Garner (3)
For DOE/TIC (Unlimited Release)
3161 J. E. Mitchell (15)
3161 P. S. Wilson
4533 J. W. Reed
4700 J. H. Scott
4710 G. E. Brandvold
4715 R. H. Braasch (200)
4715 J. D. Cyrus
4715 R. D. Grover
4715 E. G. Kadlec
4715 P. C. Klimas
4715 M. T. Mattison
4715 R. O. Nellums
4715 W. N. Sullivan
4715 R. A. Watson
4715 D. F. Wolf
4715 M. H. Worstell
5520 T. B. Lane
5523 R. C. Reuter, Jr.
5523 T. G. Carne
5523 D. B. Clauss
5523 D. W. Lobitz
5523 P. S. Veers

5600 D. B. Shuster
5620 M. M. Newsom
5630 R. C. Maydew
5633 R. E. Sheldahl
5636 J. K. Cole
5636 D. E. Berg
5636 W. H. Curry

☆ U.S. GOVERNMENT PRINTING OFFICE:1981-0-777-023/593

Org.	Bldg.	Name	Rec'd by	Org.	Bldg.	Name	Rec'd by